Submitted to ApJ.
Preprint typeset using LaTeX style emulateapj v. 6/22/04

arXiv:astro-ph/0412506v1 20 Dec 2004

DUST SENSITIVITY OF ABSORPTION-LINE INDICES

Lauren A. MacArthur
Department of Physics & Astronomy, University of British Columbia, 6224 Agricultural Road, Vancouver, BC CANADA V6T 1Z1
Submitted to ApJ.

ABSTRACT

We investigate the effects of dust extinction on integrated absorption-line indices that are widely used to derive constraints on the ages and metallicities of composite stellar systems. Typically, absorption-line studies have been performed on globular clusters or elliptical galaxies, which are mostly dust-free systems. However, many recent studies of integrated stellar populations have focused on spiral galaxies which may contain significant amounts of dust. It is almost universally assumed that the effects of dust extinction on absorption-line measurements are entirely negligible given the narrow baseline of the spectral features, but no rigorous study has yet been performed to verify this conjecture. In this analysis, we explore the sensitivity of the standard set of Lick absorption-line indices, the higher-order Balmer line indices, the 4000 Å break, the near-IR calcium triplet indices, and the Rose indices to dust absorption according to population synthesis models that incorporate a multi-component model for the line and continuum attenuation due to dust. The latter takes into account the finite lifetime of stellar birth clouds. While dust does not greatly affect the line-index measurements for single stellar populations, its effect can be significant for the 4000 Å break or when there is a significant amount of current star formation.
Subject headings: absorption-line indices, ISM: dust, extinction, galaxies: stellar content

1. INTRODUCTION

Stellar population studies play a fundamental role in our understanding of stellar evolution, initial mass functions (IMFs) associated with star cluster formation, and galaxy formation and evolution. With the aim of determining the star formation histories (SFHs) of stellar systems of all types (from star clusters to entire galaxies), many techniques have been developed, with varying success, to determine the luminosity-weighted ages and metallicities of nearby and distant stellar systems. Important caveats hinder or limit the application of these techniques (e.g. Charlot, Worthey, & Bressan 1996; MacArthur et al. 2004; Anders et al. 2004; Tantalo & Chiosi 2004). For example, the determination of ages and metallicities of stellar populations has been plagued by the well-known age/metallicity degeneracy (Worthey 1994). Access to both optical *and* infrared imaging partially lifts this degeneracy, but broad-band colors suffer further from a degeneracy due to dust reddening (e.g. Bruzual, Magris, & Calvet 1988; Witt, Thronson, & Capuano 1992; de Jong 1996; Bell & de Jong 2000; MacArthur et al. 2004), which is particularly problematic in the context of gas rich, star forming systems. Another method of breaking the age/metallicity degeneracy of stellar populations in unresolved systems involves measurement of surface brightness fluctuations (Worthey 1993; Liu, Charlot & Graham 2000; Blakeslee, Vazdekis & Ajhar 2001), which are most sensitive to contributions from the most luminous stars in the system – typically evolved cool giants. Being sensitive to the second moment of the stellar luminosity function, surface brightness fluctuations provide complementary information to the integrated colors (the first moment of the stellar luminosity function). This method, however, requires the assumption of a smooth underlying light distribution, and thus is generally only applicable to studies of nearby globular clusters, ellipticals, and spiral bulges. This broad-band technique is also not applicable to dusty systems (e.g. spiral galaxies), as the resulting clumpiness will also cause fluctuations in surface brightness and reddening will affect the fluctuation colors. Turning to spectroscopy offers the possibility of overcoming the ambiguities of broad-band color-based analyses by studying the variation of individual line strengths which, if defined over a sufficiently narrow wavelength range, should be insensitive to the effects of dust reddening. In this analysis we test this conjecture by exploring the effects of dust absorption on commonly-used spectroscopic age and metallicity indicators.

In the past three decades, tremendous progress has been made in the modeling of simple stellar populations (SSPs) (e.g. Tinsley 1972; Bruzual & Charlot 1993; Worthey 1994; Vazdekis 1999; Fioc & Rocca-Volmerange 1997; Maraston 1998; Bruzual & Charlot 2003). The current versions provide numerous observables such as high-resolution spectra, magnitudes, colors, mass-to-light ratios, and line-index measurements (including all those described above), for single bursts of star formation (SF) with a given IMF and metallicity at ages ranging from 0–20 Gyr. In particular, the Bruzual & Charlot (2003) models include a prescription for dust attenuation (described in §3) that we adopt for this analysis.

Numerous studies of absorption-line indices in the integrated spectra of composite systems have sought to disentangle and constrain the ages and metallicities of their stellar populations (e.g. Maraston & Thomas 2000; Trager et al. 2000; Schiavon et al. 2002; Caldwell, Rose, & Concannon 2003). The majority of these studies have focused on globular clusters (GCs) and elliptical galaxies, where dust is not conspicuous. Recently, however, a number of studies have turned their attention to the stellar populations of spiral galaxies, where dust is an in-

Electronic address: lauren@physics.ubc.ca

eluctable hindrance (Fisher, Franx, & Illingworth 1996; Goudfrooij, Gorgas, & Jablonka 1999; Trager, Dalcanton, & Weiner 1999; Proctor & Samson 2002; Bergmann, Jørgensen, & Hill 2003; Kauffmann et al. 2003a; Falcón-Barroso et al. 2003). Reddening by dust has often been assumed to have a negligible effect on on line indices, but no rigorous study has yet been performed to verify this conjecture. This work presents the first such analysis.

The outline of the paper is as follows; a description of the line-indices studied and their applicability as age and metallicity discriminators is given in §2. The stellar population synthesis models and dust prescription are described in §3. In §4 we discuss the dust sensitivities of the Lick & higher-order Balmer line indices, the 4000 Å break, the Ca II triplet indices, and the Rose indices, and the results are summarized in §5. Finally, in Appendix A, we present age and metallicity fits to the model galaxies in several index–index planes and discuss the errors on the derived physical parameters due to dust extinction.

2. DESCRIPTION OF INDICES STUDIED

2.1. *The Lick/IDS System*

The Lick/IDS system of 21 spectral line indices was designed to calibrate the strength of fundamental spectral features in stars and composite systems (e.g. Gorgas et al. 1993). The indices measure the strength of a particular spectral feature (either atomic and defined as an equivalent width in Å, or molecular and measured in magnitudes) relative to a pseudo-continuum on each side of the feature. The most reliable indices have been calibrated as a function of stellar color (effective temperature), surface gravity, and metallicity (Gorgas et al. 1993; Worthey et al. 1994) allowing for the construction of semi-empirical population models (e.g. Worthey 1994). The Lick indices are sensitive to the metallicity and age of stellar populations to varying degrees. When compared with population models, diagnostic plots of age versus metallicity sensitive indices, such as Hβ versus Mgb or $\langle$Fe$\rangle$, help break the age-metallicity degeneracy. However, measurements of many of the Lick indices are quite sensitive to spectral resolution and, thus, to the velocity dispersion of the system (González 1993; Trager et al. 1998; Proctor & Sansom 2002), and their use requires relatively high signal-to-noise data (S/N $\gtrsim$ 50/Å; see Cardiel et al. 1998). In addition, certain indices, Hβ in particular, can suffer "in-filling" from nebular emission contamination, present even in early-type galaxies (González 1993; deZeeuw et al. 2002; Caldwell, Rose, & Concannon 2003).

2.2. *Higher Order Balmer Indices*

In order to overcome the problem of nebular emission fill in of the Hβ feature, Worthey & Ottaviani (1997; hereafter WO97) introduced two pairs of indices that measure the higher-order Balmer lines Hγ and Hδ. Two definitions for each feature were defined, the narrower version ($\Delta\lambda \simeq 20$ Å) is denoted with the subscript "F" (as it encompasses all of the Balmer line absorption from stars of spectral type F at the Lick/IDS resolution of 8–10 Å), e.g. Hδ_F, and the wider definition ($\Delta\lambda \simeq 40$ Å) has the subscript "A" (as it includes all of the absorption from A stars), e.g. Hγ_A. The narrow indices are more age-sensitive, but require higher S/N and resolution. While their age-sensitivity is not as strong as for Hβ, the higher-order Balmer lines are much less affected by emission from ionized gases (e.g. Osterbrock 1989). Thus, when combined with a metallicity sensitive index, the WO97 indices provide a more reliable age estimate for star-forming galaxies. Note, however, that the WO97 higher-order Balmer lines are poorly calibrated (Vazdekis 1999), likely due to the degrading resolution at the blue end of the IDS data.

2.3. *The 4000 Å Break*

Another widely used spectral index that obviates the need for high S/N and spectral resolution is the 4000 Å break, a flux ratio that brackets the strongest discontinuity in the optical spectrum of a galaxy. The break arises due to the accumulation of a large number of spectral lines in a narrow wavelength region bluewards of 4000 Å in stellar types cooler than G0 (Bruzual 1983; Gorgas et al. 1999). The main contribution to the $\lesssim$ 4000 Å opacity comes from atomic metals (Fe I, Mg I, Ca II) and molecular CN, which decreases for hotter and more metal poor stars. Thus the 4000 Å break is weak for young and/or metal-poor stellar populations and strong for old, metal-rich galaxies (Kauffmann et al. 2003a). In its original form, (Bruzual 1983), the 4000 Å break, denoted D(4000), was defined as the ratio of the average fluxes per frequency unit measured over the spectral ranges 4050–4250 Å and 3750–3950 Å. Cardiel et al. (1998) demonstrated that this discontinuity can be measured with a relative error of $\sim$ 10% with a S/N per Å $\sim$ 1, thus making it better suited for lower quality data. However, the D(4000) does have a few drawbacks due to its long baseline. These were partially alleviated with the introduction of a narrower definition (Balogh et al. 1999) denoted $D_n(4000)$ and measured over the ranges 4000–4100 Å and 3850–3950 Å. The narrow definition was designed to exploit two principal advantages: an improved agreement between multiple measurements of a given galaxy, and a weaker sensitivity to reddening effects. However, using their narrow $D_n(4000)$ index, Balogh et al. (1999) still had to invoke dust reddening as a cause for the large $D_n(4000)$ values in a number of their $z \sim 0.3$ galaxies, i.e. $D_n(4000)$ is not impervious to dust effects. Nevertheless, often found in the literature is the statement that the $D_n(4000)$ is *insensitive* to dust attenuation effects. For example, Kauffmann et al. (2003b) use the amplitude of the $D_n(4000)$ in combination with the strength of the Hδ_A index of WO97 as diagnostics for the SFH of the host galaxies, from which they infer the dust attenuation by comparing observed to model colors, a method that relies heavily on the assumption of dust insensitivity of the $D_n(4000)$ and Hδ_A indices.

2.4. *The Near-IR Ca II Triplet Indices*

There has been a great effort recently to extend stellar population studies to the near-IR region, focusing on the Ca II triplet as one of the most prominent features in the near-IR spectrum of cool stars (from spectral types of about F5 to M2) (Cenarro et al. 2001a,b; Vazdekis et al. 2003). Three "Lick-style" indices designed to measure the strengths of the Ca II triplet lines ($\lambda\lambda$8498.02, 8542.09, 8662.14 Å), and denoted Ca1, Ca2, and Ca3, have been defined and redefined by several authors (e.g.

Jones, Alloin, & Jones 1984; Armandroff & Zinn 1988; Diaz, Terlevich, & Terlevich 1989, hereafter DTT; Delisle & Hardy 1992). However, measurement of a reliable continuum for these indices is difficult due to the strong and crowded absorption features in the vicinity of the Ca II lines (largely from Fe I, Mg I, and TiO), as well as significant blending with the hydrogen Paschen series whose absorption is present in stars of types G3 and hotter.

To overcome these problems, Cenarro et al. (2001a) defined a new set of Ca II triplet indices specifically designed for measurement in integrated galactic spectra. The new definitions are categorized as "generic" indices, which have advantages over the classical "Lick-style" indices when looking at adjacent absorption lines in regions where the continuum is crowded with spectral features. Their CaT index includes the strenghts of all three Ca II lines and uses a combination of 5 continuum bandpasses (see Cenarro et al. 2001a for details on the measurement of generic indices). Additionally, they define the generic index PaT, which measures the strength of three of the H Paschen series lines that are free from Ca contamination. Finally, the index CaT* is designed to remove the H Paschen line contamination from CaT making it a reliable indicator of the pure Ca II triplet strength. The index is given by CaT* = CaT - 0.93 PaT. Vazdekis et al. (2003) discuss the behavior of these features for SSPs as predicted by recent evolutionary synthesis models. In the current analysis we also explore the dust sensitivity of the three classical Ca II triplet indices, as defined in DTT, and the generic indices of Cenarro et al. (2001a).

2.5. *The Rose Indices*

The optical Rose (1984, 1985) indices were developed in part to overcome the difficulties in identifying the continuum in crowded spectral regions. The Rose indices maximize the contribution of a given feature by using a measurement of the ratio of its central line intensity to that of a close reference line, without recourse to the (pseudo-) continuum level. Information about equivalent widths is however lost in such relative measurements, and the Rose indices are not ideal for separating age and metallicity effects. Nonetheless, some of the Rose indices are quite sensitive to metallicity (see Vazdekis 1999) and, in combination with a sensitive age indicator (e.g. Hβ), could help disentangle the two effects. The Rose indices also provide a unique and sensitive test for the presence of early-type stars (i.e. a post-starburst, and potentially dusty, population) in an integrated spectrum as well as a probe of the relative contribution of dwarf and evolved (red giant branch) stars to the integrated spectrum of a galaxy (Caldwell, Rose, & Concannon 2003). As with the Lick indices, it is usually assumed that the Rose indices are insensitive to dust reddening (e.g. Leonardi & Worthey 2000), an assumption we examine in this study.

Finally, we also investigate dust effects on the pseudo-equivalent width, "Lick-style", indices of Rose (1994) and Jones & Worthey (1995) which have extremely narrow definitions (and are denoted with the subscript "HR"). The H$\gamma_{\rm HR}$ index has been identified as one of the most sensitive age distriminators (Jones & Worthey 1995), but these narrow features suffer a worse resolution sensitivity than the WO97 indices and thus can only be used with high quality data of low velocity-dispersion systems. Vazdekis & Arimoto (1999) and Vazdekis et al. (2001) confronted the velocity dispersion sensitivity of these narrow indices by defining a set of four Hγ indices that take resolution effects into account, allowing for reliable measurements in galaxies with velocity dispersions up to $\sigma \sim 300$ km s^{-1}. Note, however, that the Vazdekis & Arimoto (1999) indices require S/N > 200–400/Å and have strong error covariances due to overlapping pseudo-continuum and central bandpasses, making them much harder to measure than the WO97 indices. The response of these indices to dust extinction is similar to the WO97 Hγ_F and the Jones & Worthey (1995) H$\gamma_{\rm HR}$ indices, so the results are not shown.

3. MODELS

The stellar population synthesis models used for this analysis are those of Bruzual & Charlot (2003; hereafter GALAXEV). The high resolution models using the Padova evolutionary tracks (Bertelli et al. 1994) and the Chabrier (2003) IMF were adopted. These models include SSP spectra in the wavelength range 3200–9500 Å with a resolution of 3 Å, metallicities ranging from $Z =$ 0.0001–0.05 (or 0.005–2.5 times $Z_\odot$), and ages ranging from 0–20 Gyr (in 220 unequally-spaced time steps). For each time step, a number of integrated quantities are provided such as magnitudes and colors in many different filter systems, line-index strengths for all definitions in the Lick/IDS system, WO97, the two definitions of the 4000Å break, and the DTT Ca II indices. The line strengths used here are computed directly from the high-resolution model spectra, i.e. the spectra have not been transformed to the Lick/IDS system (see e.g. WO97). The Rose, Ca II, and "HR" spectral indices, which are not provided with the BC03 model outputs, were computed with a public `fortran` program by A. Vazdekis[1].

The GALAXEV distribution allows for the computation of attenuation effects due to dust according to the two-component model of Charlot & Fall (2000; hereafter CF00). The two adjustable parameters of this model are $\hat{\tau}_V$, the total effective V-band optical depth affecting stars younger than 10^7 yr, and μ, the fraction of the total dust absorption contributed by diffuse interstellar medium (cirrus) dust. That is,

$$\hat{\tau}_\lambda = \begin{cases} \hat{\tau}_V(\lambda/5500\ \text{Å})^{-0.7} & \text{for } t \le 10^7 \text{ yr}, \\ \mu\,\hat{\tau}_V(\lambda/5500\ \text{Å})^{-0.7} & \text{for } t > 10^7 \text{ yr}, \end{cases} \quad (1)$$

where t is the age of any single stellar generation. This model has the singular feature of accounting for the finite lifetime ($\sim 10^7$ yr) of stellar birth clouds[2]. The wavelength dependence of the effective absorption curve (proportional to $\lambda^{-0.7}$) was constrained to reproduce the observed relation between the ratio of far-infrared to ultraviolet luminosities, and the ultraviolet spectral slope of their starburst galaxies (see also the GRASIL models of Silva et al. 1998). Note that $\hat{\tau}_\lambda$ on the left-hand side of equation (1) is a function of time and μ. As a result, even if $\mu = 0$ (no cirrus dust component), in the presence of young stellar populations ($t \le 10^7$ yr), dust will still contribute some extinction (see Fig. 1). Note that in the adopted dust model of CF00, the model spectra are

[1] See http://www.iac.es/galeria/vazdekis/

[2] Introduced to resolve the apparent conflict between the attenuation of line and continuum photons in their sample of starburst galaxies.

representative of the total integrated light of a galaxy, i.e., neither radial nor inclination dependent information is available.

Other prescriptions for dust attenuation in galaxies exist (e.g. Witt, Thronson, & Capuano 1992; Byun, Freeman, & Kylafis 1994; de Jong 1996; Gordon et al. 2001), a few of which have been coupled with spectral synthesis and photo-ionization codes. For example, Moy et al. (2001) interfaced the PÉGASE population synthesis models of Fioc & Rocca-Volmerange (1997) with the CLOUDY photo-ionization code of Ferland (2002). These models include a treatment for dust attenuation processes, but do not consider nebular emission. They also adopt a simple screen approximation for the dust distribution, an unrealistic geometry for galaxies. Similarly, Panuzzo et al. (2003) coupled the same CLOUDY code with their spectrophotometric synthesis model GRASIL (Silva et al. 1998), to yield a complete treatment of dust reprocessing with more realistic geometries and account for the age dependence of molecular birth clouds (as in CF00). While these models may be more realistic and provide directional information that is lacking in the CF00 models, the resolution of the output from these models is not sufficient for accurate line-index measurements. Future implementations of these models may allow for a comparative analysis, but at present, the CF00 dust models, coupled with the BC03 SPS models, provide (to the best of our knowledge) the only suitable output for the current study.

In a study of 705 non-Seyfert galaxies drawn from the Stromlo-APM redshift survey (Loveday et al. 1996), Charlot et al. (2002) determined parameters for the CF00 models that reproduce the observed integrated spectral properties of the nearby star-forming galaxies. These cover the ranges: $0.2 \leq Z/Z_{\odot} \leq 4.0$, $0.01 \leq \hat{\tau}_V \leq 4.0$, and $0.2 \leq \mu \leq 1.0$, for constant and exponential SFHs with ages 10^7 yr $\leq t \leq 10^{10}$ yr. Two time-scales were adopted for the exponentially declining star formation rate: $\tau_{exp} = 0.1$ and 6.0 Gyr. Our model realizations cover roughly the same parameter space. For the SSP models we consider values of $\mu = 0$ and 1 only since, for the SSP ages shown ($t > 10^7$ yr), different values of μ are equivalent to different values of $\hat{\tau}_V$. For the exponential SFHs, for which there are always populations with $t \leq 10^7$ yr present, we present models with $0 < \mu < 1$ and extend to $\hat{\tau}_V = 8$ (so for the $\mu = 0.3$ case, the plots effectively extend to $\hat{\tau}_V = 2.4$). To express the effective dust reddening in a more familiar form, in Figure 1 we plot the color excesses $E(B-V)$ and $E(V-K)$ as a function of $\hat{\tau}_V$ resulting from the dust models used in this analysis. The upper panels are for solar metallicity SSPs with $\mu = 0.0$ (circles) & 1.0 (triangles) and the lower panels show exponential SFH with $\tau_{exp} = 13$ Gyr for $\mu = 0.0$ (circles), 0.3 (triangles), & 0.9 (squares) at ages of 0.5 (dotted lines; red shades), 5 (dashed lines; green shades), & 13 Gyr (solid lines; blue shades).

Before examining the response of the individual indices to the dust reddening, it is useful to look at the spectral energy distribution (SED) of the models. Figure 2 shows the model SEDs in the 3700–6700 Å range for SSPs [left panels] and exponential SFHs with $\tau_{exp} = 13$ Gyr [right panels]. All spectra have been normalized to 5500 Å. The SSP SEDs look entirely as expected, with the 0.5 Gyr population [top right panel] closely resembling an early-type (A–F) stellar spectrum with a blue continuum, strong Balmer features, but few metallic features. The 13 Gyr spectrum [bottom right panel] more closely resembles a later-type (G–K) stellar spectrum with a redder continuum, weaker Balmer-line strengths, and more metallic absorption features. In both cases, the dust extincted profiles exhibit the overall low frequency reddening of the SED due to the $\lambda^{-0.7}$ dependence of the dust model. On the other hand, the unreddened 0.5 Gyr SED for an exponential SFH with $\tau_{exp} = 13$ Gyr (Fig. 2 [top right panel, black curve]) is even bluer than its SSP counterpart because of the presence of young stars (< 0.5 Gyr) from the ongoing SF. The contrast between the SSP and exponential SFHs is even more striking at 13 Gyr. The exponential SFH SED (Fig. 2 [bottom right panel, black curve]) is much bluer than its SSP counterpart [bottom left panel] due to the ongoing SF, but it also shows metallic features due to the presence of older stars (≤ 13 Gyr). In the exponential SFH case, the dust reddening is more complicated due to the presence of young stars that still live in their birth clouds ($< 10^7$ yr). These stars are more extincted than the older stars, the cirrus extinction component, when $\mu < 1.0$, but being intrinsically bright, still contribute significantly to the total flux. In Figure 2 [right panels] we show the case for $\mu = 0.3$. Clearly, any measurement made over a long baseline (e.g. colors) will be affected by the dust reddening. However, gauging its effects on absorption-line indices from a cursory examination of the SEDs is not a straightforward task. In the next section we examine individual features and compare the dust-free indices with those computed with dust.

4. RESULTS

4.1. *Dust Sensitivity of the Lick Indices*

The response of the Lick indices as a function of $\hat{\tau}_V$, μ, and age for solar metallicity ($Z_{\odot} = 0.02$) and abundance ratio ([α/Fe] = 0) SSP models is shown in Figure 3. In each panel, we plot $\Delta index$ versus $\hat{\tau}_V$, where $\Delta index$ is the difference between the indices measured with and without dust (for the same age & SFH), i.e. $\Delta index \equiv index(\hat{\tau}_V) - index(\hat{\tau}_V = 0)$. Results are shown for model ages of 0.5 (dotted lines; red shades), 5 (dashed lines; green shades), & 13 Gyr (solid lines; blue shades). The two values for μ of 0.0 & 1.0 are denoted by circles and triangles, respectively. The horizontal dotted lines in Figures 3, 4, & 7 – 11 denote typical measurement errors for the different indices; $\sim$ 0.1 Å for the atomic Lick indices, 0.01 mag for the molecular Lick indices, 0.4 Å for the WO97 indices, 0.03 for D(4000) and $D_n(4000)$, and $\sim$0.02–0.05 for the Rose indices (Gorgas et al. 1999; Jones & Worthey 1995; Kauffmann et al. 2003a; Falcón-Barroso et al. 2003; Caldwell, Rose, & Concannon 2003; J.J. González 2004, private comm.), and serve as a guide for the magnitude of the effect from dust required to be detectable above the noise. All model realizations presented here have solar metallicity, $Z_{\odot} = 0.02$. We have also considered the other metallicities in the GALAXEV models. Generally, the dust effects are slightly more conspicuous at $Z = 0.05$, but diminish with decreasing metallicity of the stellar population.

In most cases, the index measurements do not devi-

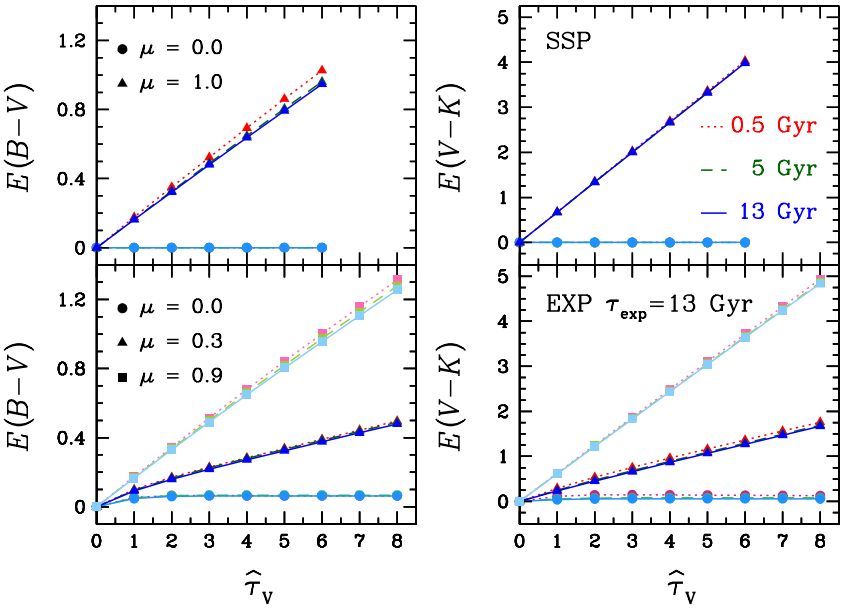

FIG. 1.— Color excesses $E(B-V)$ [left panels] and $E(V-K)$ [right panels] as a function of $\hat{\tau}_V$ for solar metallicity SSPs with $\mu = 0.0$ (circles) & 1.0 (triangles) [top panels] and an exponential SFH with $\tau_{exp} = 13$ Gyr for $\mu = 0.0$ (circles), 0.3 (triangles), and 0.9 (squares) [bottom panels]. Different ages are represented by: 0.5 (dotted lines; red shades), 5 (dashed lines; green shades), & 13 Gyr (solid lines; blue shades).

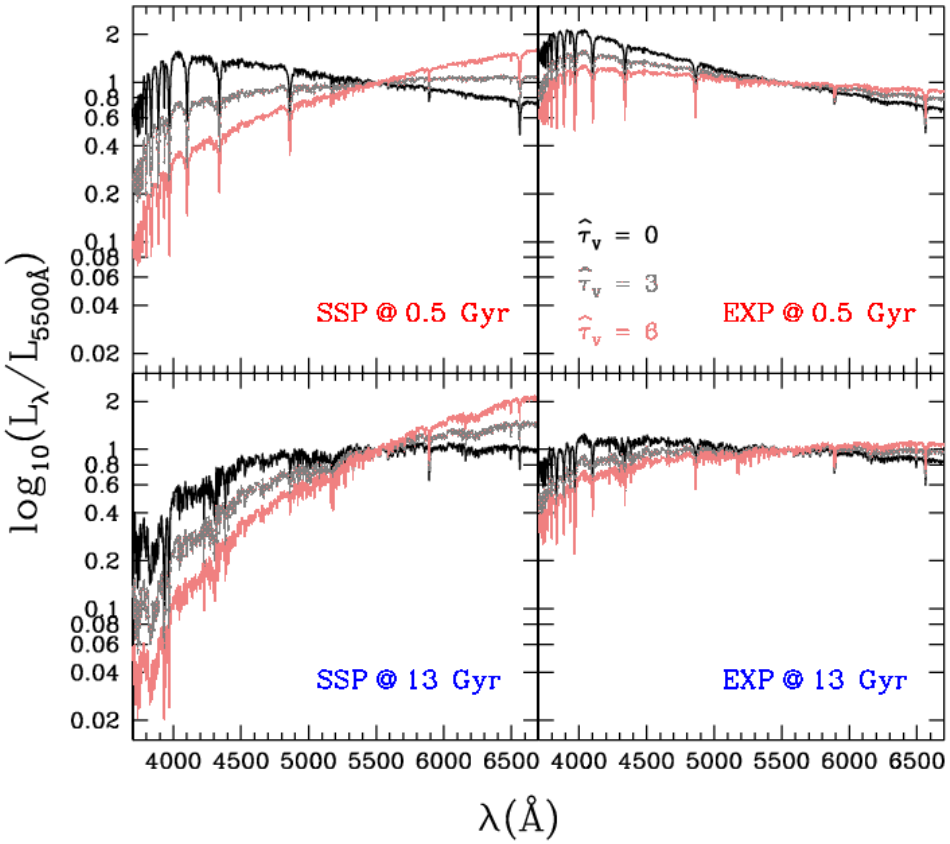

FIG. 2.— Comparison of solar metallicity SEDs with $\hat{\tau}_V = 0$ (black), 3 (gray), & 6 (pink) at ages of 0.5 [top panels] & 13 Gyr [bottom panels] for SSP models with $\mu = 1.0$ [left panels] and exponential SFH models with $\tau_{exp} = 13$ Gyr and $\mu = 0.3$ [right panels].

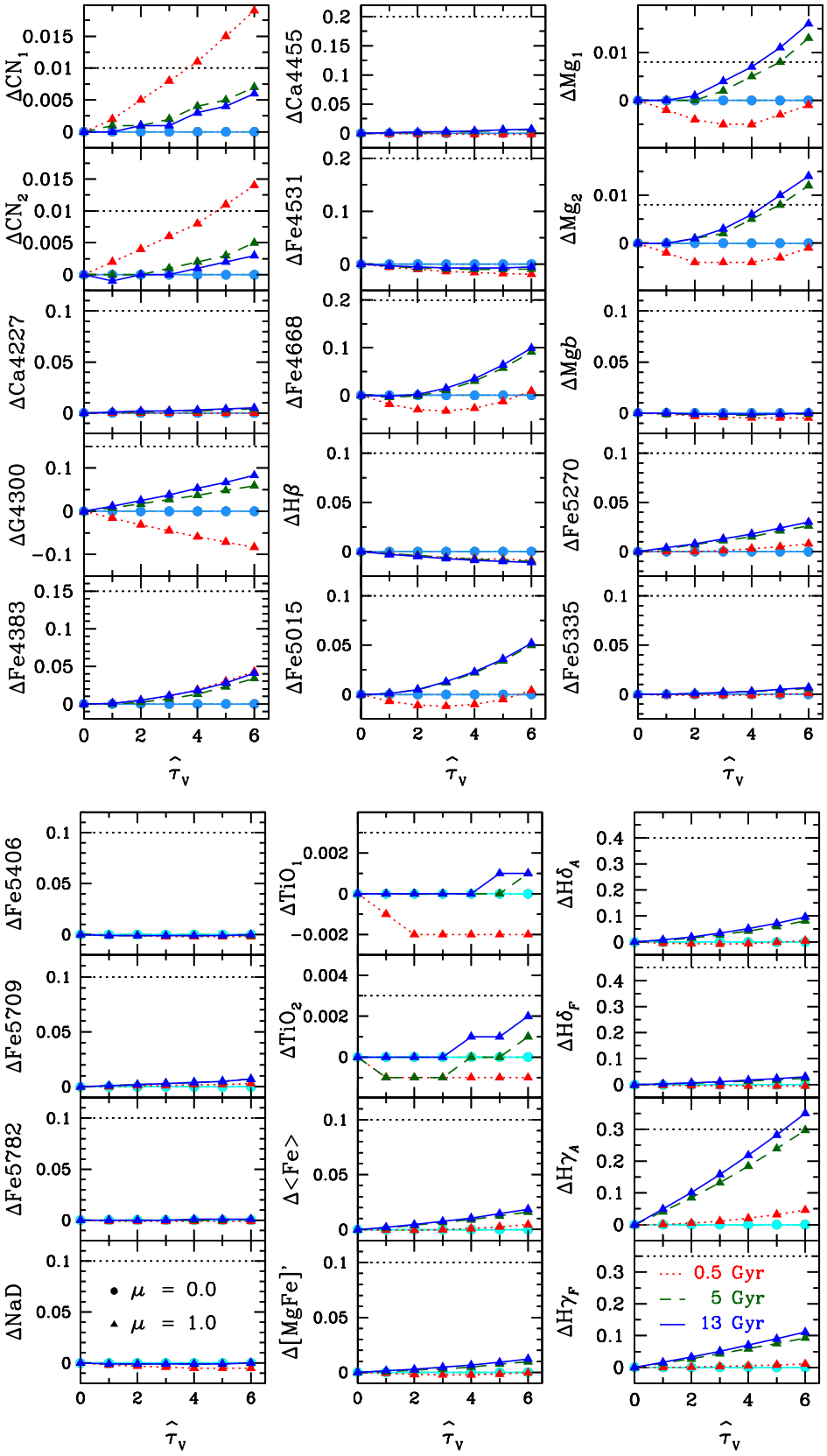

FIG. 3.— Lick and WO97 index differences, $\Delta index \equiv index(\hat{\tau}_V) - index(\hat{\tau}_V = 0)$, as a function of $\hat{\tau}_V$ for solar metallicity SSPs. Different ages are represented by: 0.5 (dotted lines; red shades), 5 (dashed lines; green shades), & 13 Gyr (solid lines; blue shades). Different values of μ are represented as 0.0 (circles), and 1.0 (triangles). The black horizontal dotted lines represent typical measurement errors for the different indices.

ate considerably from their dust-free values in the SSP models, as expected. Since we consider SSPs at ages of 0.5 Gyr and greater, by definition, models with $\mu = 0$ have no dust extinction (thus circle symbols lie at 0 for all values of $\hat{\tau}_V$ in Fig. 3). For $\mu = 1$ models, deviations from the dust-free index measurements do occur. There are a few cases of note that show significant sensitivity to the dust extinction, such as the molecular indices Mg_1 & Mg_2, and CN_1 & CN_2. This is not surprising since these indices have the longest wavelength baseline ($\Delta\lambda \sim$400 & 200 Å respectively). As evidenced by the molecular Mg indices, index measurements in the presence of dust can be non-linear and age dependent, thus a simple "dust-correction" poses a formidable challenge. The effect of extinction on the Mg indices goes in the opposite direction for young ages as it does for older ages (compare dotted and dashed/solid lines in Fig. 3). Also, the CN indices are more severely affected at younger ages whereas the Mg indices are more affected at young ages for small $\hat{\tau}_V \lesssim 3$, but at older ages for larger $\hat{\tau}_V > 4$.

Of the Lick atomic indices, those showing the greatest sensitivity to dust are Fe5015 & Fe4668, both having the longest wavelength baselines of all atomic indices, but their deviations from the dust-free case are always smaller than the typical measurement errors. In addition to the standard Lick indices, we also show the combination indices, $\langle$Fe$\rangle$= (Fe5270+Fe5335)/2 and [MgFe], first introduced by González (1993). For the latter we use the slightly modified definition of Thomas, Maraston, & Bender (2003), $[\mathrm{MgFe}]' = [\mathrm{Mg}b(0.72{*}\mathrm{Fe5270}{+}0.28{*}\mathrm{Fe5335})]^{1/2}$, which has the advantage of being completely independent of the element abundance ratio ([α/Fe]). These combination indices vary very little with $\hat{\tau}_V$ for the SSP models (Fig. 3).

The higher-order Balmer indices, shown in Figure 3, also show some sensitivity to dust at older ages in the SSP models, particularly the Hγ_A index. Measurement errors for these indices are quite large compared to the other Lick indices (due to their narrow baselines), thus any reddening effect would likely not be detectable.

Unlike GCs and elliptical galaxies, the assumption of SSP-like star formation is clearly not applicable for spiral galaxies. While the true SFHs of the latter are poorly known in detail, they are often approximated with an exponentially declining SFR, parameterized by a star formation timescale τ_{exp} (e.g. Bell & de Jong 2000; MacArthur et al. 2004). In Figure 4 we show the index responses to dust for an exponential SFH with $\tau_{exp} = 13$ Gyr, which is reasonably close to a constant SF rate so there is a significant amount of "current" SF at each of the three epochs considered.

Models with current SF yield considerably different results than the SSPs, as seen in Figure 4. Almost all of the Lick indices show sensitivity to dust, some more so at young ages (e.g. CN_1, CN_2, Hβ, and all four WO97 indices), others more so at older ages (e.g. Ca4227, Fe4531, Fe4668, Mgb, and NaD), and some show differences of equal magnitude, but in opposite directions at old and young ages (e.g. G4300, Fe4383, and the molecular Mg indices). The situation is undoubtedly complex and can be attributed to the fact that, with current SF occurring at all epochs, there is a significant and non-linear amount of extinction of the hottest, youngest stars which contribute considerably to the total optical flux. As such, dust effects are often stronger for models with smaller μ and these effects saturate at optical depths above about $\hat{\tau}_V = 3$ (at which the birth clouds become completely optically thick).

The situation for mixed stellar populations with significant amounts of current SF is clearly complicated and not easily prescribed. However, for many of the indices (e.g. Ca4227, Ca4455, Fe5406, Fe5709, Fe5782, NaD, TiO_1, and TiO_2), the magnitude of the dust effects is never close to that of current typical measurement errors, and thus would not be detected. Unfortunately, however, the most often used indices (e.g. Hβ, Mgb, the composite indices $\langle$Fe$\rangle$ and [MgFe]$'$, and the WO97 indices) are also the most seriously affected.

It is useful to take a closer look at the cause for the erratic behavior in some of the indices in response to the dust extinction. In Figure 5 we focus on the Hβ index. Plotted in each panel are solar metallicity SEDs for $\hat{\tau}_V$ = 0 (black), 3 (gray), & 6 (pink) at ages of 0.5 [top panels], & 13 Gyr [bottom panels]. The index red and blue pseudo-continuum band limits are marked by the green dashed vertical lines and the central band by the solid vertical lines. The dotted lines mark the pseudo-continuum level for each spectrum. The spectra are all normalized to their 4861 Å flux (Hβ line center). Figure 5 plots SSPs [right panels] with $\mu = 1.0$ exponential SFHs [left panels] with $\mu = 0.3$. There is very little effect in the SSP index measurement, the change in slope of the SED is matched by the change in slope of the pseudo-continuum. However, for the exponential SFH at 0.5 Gyr (Fig. 5 [top right panel]), the continuum is increased relative to the depth of the absorption-line in the dust extincted models. This can be understood by recognizing that the young OB stars that suffer significant extinction have lower Hβ values. Thus, by hiding these low Hβ index stars, the index is effectively increased. In fact, this is the case for all of the Balmer lines, hence all of the Balmer-line indices show similar behavior. This also highlights a major limitation when using Balmer-line indices in determining young ages ($\lesssim$ 0.5 Gyr). The models become degenerate in age here because there are two possible ages that can be inferred at these Balmer index values, i.e. the Balmer indices are double-valued in the region of young stellar population ages. This point and its resulting limitations are further emphasized in Appendix A.

For the molecular indices, which have much broader baselines and crowding of spectral lines in their passband regions, the situation can be more complicated. For instance, in Figure 6 we focus on the Mg_1 index. The color codes, line-types, and SFHs are the same as in Figure 5. In this case, given the much broader baseline, the slope of the pseudo-continuum in the extincted models changes quite dramatically. In the 0.5 Gyr SSP (Fig. 6 [top left panel]) and 13 Gyr exponential SFH (Fig. 6 [bottom right panel]) cases it changes from being a negative slope in the dust-free model (black) to positive in the most extincted curve (pink). These pseudo-continua pass through a crowded set of absorption lines in the central passband, and a simple inspection of these figures does not reveal which model would yield larger index measurements. It is clear from these figures that a simple dust correction prescription for all of the indices is cannot be

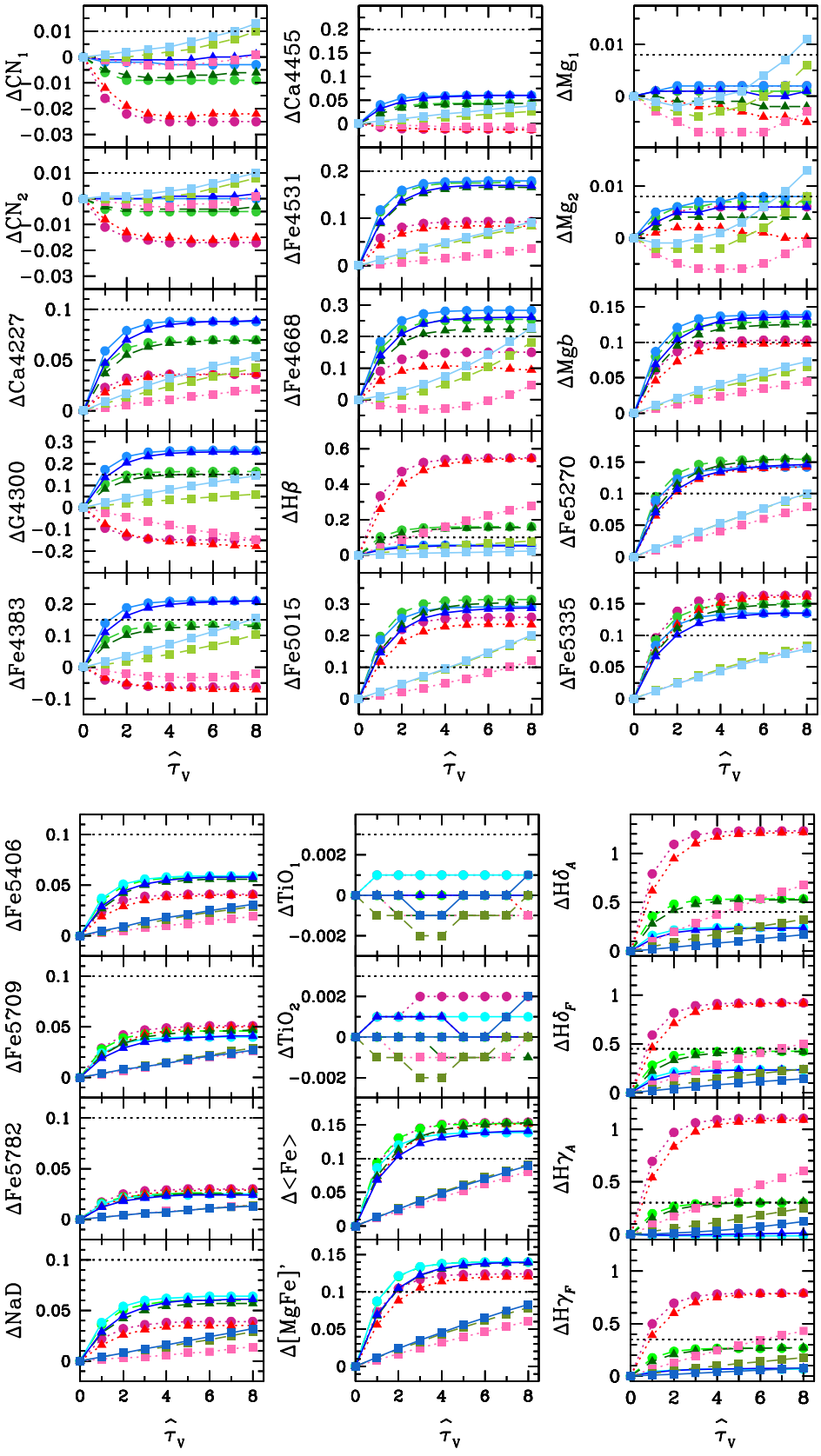

FIG. 4.— Same as Figure 3 but for for an exponential SFH with τ_{exp} = 13 Gyr and values of μ are represented as 0.0 (circles), 0.3 (triangles), and 0.9 (squares).

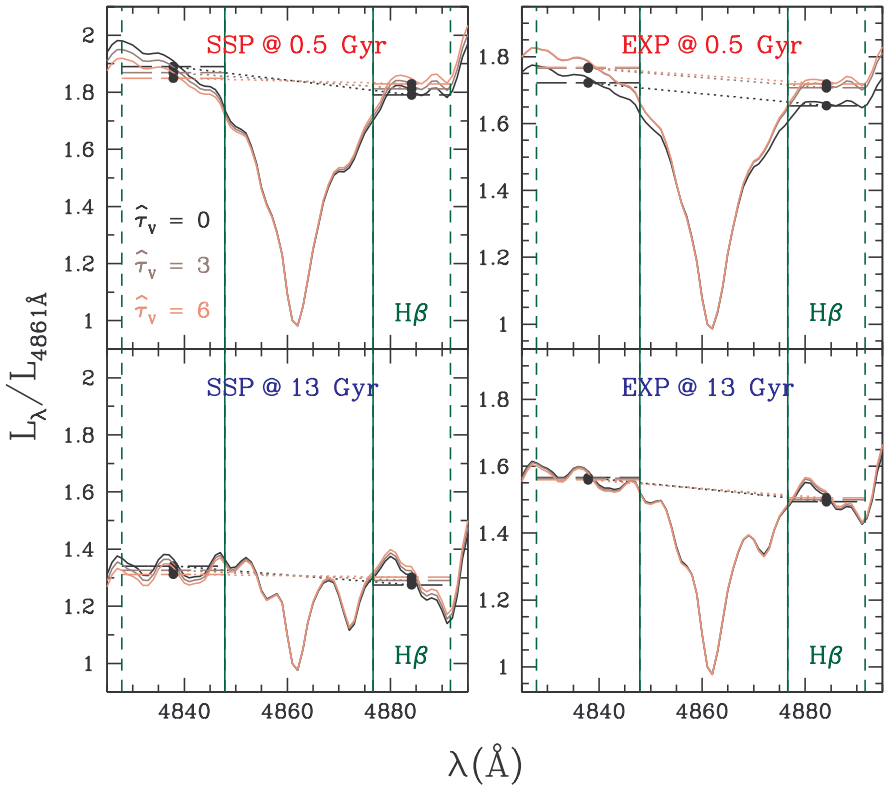

FIG. 5.— Comparison of the Hβ index for solar metallicity SSP models with $\mu = 1.0$ [left panels], and exponential SFH $\tau_{exp} = 13$ Gyr models with $\mu = 0.3$. [left panels]. All panels show models with $\hat{\tau}_V = 0$ (black), 3 (gray), & 6 (pink) at ages of 0.5 [top panels] & 13 Gyr [bottom panels]. The index red and blue pseudo-continuum band limits are marked by the green dashed vertical lines and the central band by the solid vertical lines. The dotted lines mark the pseudo-continuum level for each spectrum. The spectra are all normalized to their flux at 4861 Å (the center of the Hβ line).

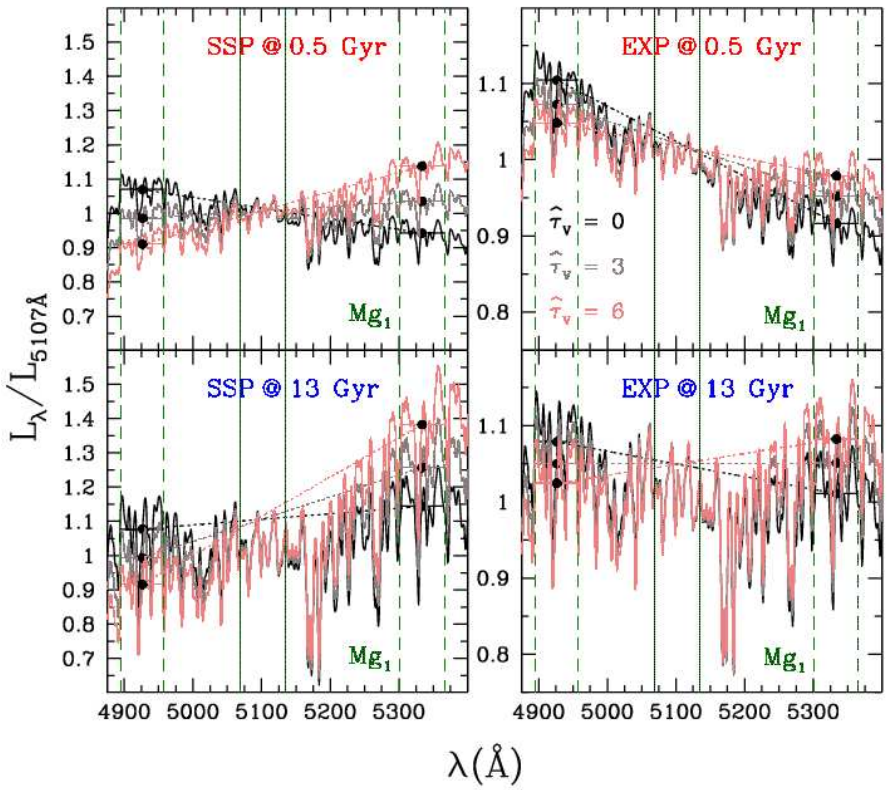

FIG. 6.— Same as Figure 5 but for Mg_1. The spectra are all normalized to their flux at 5107 Å (roughly the center of the index central passband).

achieved.

4.2. *Dust sensitivity of the 4000Å Break*

Figure 7 shows the response of D(4000) [top panels] and $D_n(4000)$ [bottom panels] to attenuation from dust for SSPs [left panels] and exponential SFHs with $\tau_{exp} =$ 13 Gyr [right panels]. The narrower index is certainly less affected by dust (note the different y-axis scales), but it is by no means impervious to dust reddening effects, and can reach deviations with magnitudes much larger than the typical error for this index. Dust effects are smaller at younger ages, but they can be significant at all ages for realistic values of $\hat{\tau}_V$. A detailed discussion of the influence of these dust effects on the determination of ages and metallicities is deferred to appendix A.

Gorgas et al. (1999) suggest that D(4000) could be corrected for the effects of internal reddening according to,

$$\mathrm{D}(4000)_{\mathrm{corrected}} = \mathrm{D}(4000)_{\mathrm{observed}} * 10^{-0.0988E(B-V)}, \quad (2)$$

derived using the mean extinction curve from Savage & Mathis (1979). However, this assumes that the dust is distributed as a screen, which is likely unrealistic for galaxies (e.g. Witt, Thronson, & Capuano 1992), and that the value of the color excess $E(B-V)$ is known. Even knowing $E(B-V)$, as we do for these models, the above formula does not reproduce the dust-free D(4000) value for the CF00 dust model. The numerical constant in equation (2) could be adjusted to obtain a good fit, but this number is a function of age, depends on the dust properties, and requires *a priori* knowledge of $E(B-V)$. Hence, we do not explore this putative correction further, but note that, as we concluded for the Lick indices, there is likely no such simple dust correction for the 4000 Å break of mixed stellar populations and complex dust geometries.

4.3. *Dust Sensitivity of the Ca II Triplet Indices*

The response of the Ca II triplet indices of DTT and Cenarro et al. (2001a) as a function of $\hat{\tau}_V$, μ, and age for solar metallicity SSP models are shown in Figure 8 and for an exponential SFH with $\tau_{exp} = 13$ Gyr in Figure 9. The three classical Lick-style Ca indices of DTT (left) show some sensitivity to dust extinction for the SSPs, Ca3 showing the largest sensitivity, but the deviations remain below the typical measurement errors thus would not be detected. The generic CaT indices (right) are virtually unaffected by dust extinction in the SSP models at any age. As usual, the situation is not as straightforward for the exponential SFH (Fig. 9). Here, the only index that is not significantly affected is the Ca1 index of DTT. All of the generic indices of Cenarro et al. (2001a) are significantly altered due to dust extinction, particularly at young ages. As in the case for the Lick indices in the exponential SFH models (§4.1, Fig. 4), dust effects are often stronger for models with smaller μ and the effects saturate at optical depths above about $\hat{\tau}_V = 4$. In general, though, for models that do not have significant amounts of current SF, the dust reddening effects in the Ca II triplet indices are still small compared to measurement errors, and should not cause problems in their interpretation.

4.4. *Dust Sensitivity of the Rose Indices*

The response of the Rose (1984, 1994) and Jones & Worthey (1995) indices are shown in Figure 10 for SSPs and in Figure 11 for an exponential SFH with $\tau_{exp} = 13$ Gyr. Symbols and line types are as in Figures 3 & 4. For SSP models there are a few indices that are considerably modified by dust reddening, namely the Hδ/Fe Iλ4045, Hδ/Fe Iλ4063, Sr II/Fe Iλ4045, Hγ/Gband, and Ca II indices, particularly at older ages. All other indices, including the pseudo-equivalent width indices, are essentially unaffected by the dust reddening in the SSPs at any age. For the exponential SFH, shown in Figure 11, the response of the indices gets quite complicated. The offset from the dust-free case can be either positive (typically for the older models) or negative (typically for youngest models). Again, for the $\mu = 0.0$ models and for some of the $\mu = 0.3$ models, the index offsets saturate for optical depths above $\hat{\tau}_V = 3$. Ultimately though, even with current SF, for the majority of the Rose indices, the index offsets due to dust reddening are modest. On the other hand, with a significant amount of current SF, the pseudo-equivalent width indices can be quite affected, more so at young ages for $\mathrm{H}\gamma_{\mathrm{HR}}$, but more so for old ages for Ca I_{HR} and Fe I_{HR}. The "HR" indices are virtually unaffected for SSP models at all ages.

5. DISCUSSION

As an illustration of the potential dangers of dust extinction when using absorption-line indices to determine ages and metallicities of star forming galaxies, in Figure 12 we present model tracks for the Lick Hβ versus $\langle$Fe$\rangle$ diagnostic plot for the dust-free exponential SFH with $\tau_{exp} = 13$ Gyr for $Z = 0.0004$, 0.02, and 0.05 (gray curves). The circles are the index values for the same SFH, but with dust extinctions ranging from $\hat{\tau}_V = 0$ (largest point size) to $\hat{\tau}_V = 8$ (smallest point size). There is virtually no error for old and metal-poor galaxies, but significant problems can arise at higher metallicities. For example, the location in the Hβ versus $\langle$Fe$\rangle$ plane for a solar metallicity stellar population at any age with $\hat{\tau}_V = 1$ lies closer to the $Z = 0.05$ model curve. The age errors are not significant in this case, but as extinction increases, the data points lie significantly outside the region covered by the model grids.

However, since in reality we don't know the true SFH of a galaxy, what is often computed are "SSP-ages and metallicities", i.e., the values that would be measured if a given index–index combination is fit to SSP model grids. In order to gauge the magnitude of the errors on SSP ages and metallicities due to dust extinction, we fit the model galaxies to SSP grids of different index–index combinations. The error on the derived parameters is taken as the difference between the fit for the dusty model and the corresponding dust-free model (i.e. ΔA = Age($\hat{\tau}_V$) − Age($\hat{\tau}_V = 0$)). In some cases we encounter difficulties with the models with current SF, as these models can lie off the SSP model grids, even in the dust-free models. Additionally, due to the double-valued nature of the Balmer lines at young ages (discussed in §4.1), there is an additional degeneracy for points that lie in the youngest region of the SSP model grids. This was the case for all of the exponential SFH models at 0.5 Gyr, for which a large fraction of the stars are very young. Details of the fits and tables providing the resulting age and metal-

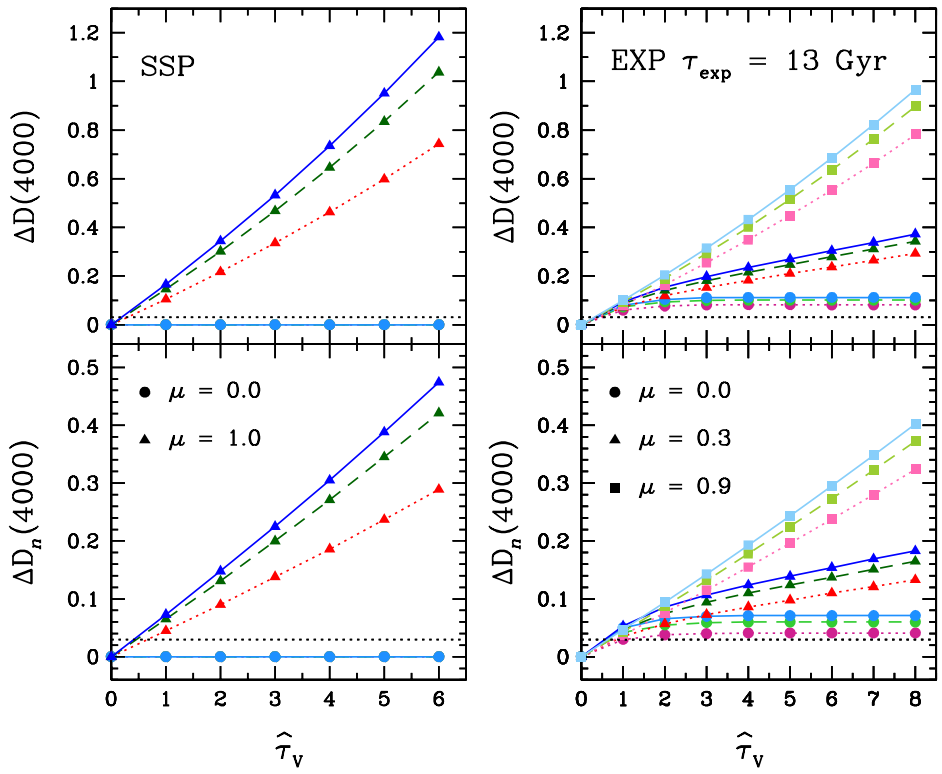

FIG. 7.— D(4000) [top panels] and D$_n$(4000) [bottom panels] differences, $\Delta index \equiv index(\hat{\tau}_V) - index(\hat{\tau}_V = 0)$, as a function of $\hat{\tau}_V$ for SSPs [left panels] and for an exponential SFH with $\tau_{exp} = 13$ Gyr [right panels]. Different ages are represented by: 0.5 (dotted lines; red shades), 5 (dashed lines; green shades), & 13 Gyr (solid lines; blue shades). The black horizontal dotted lines represent the typical measurement error.

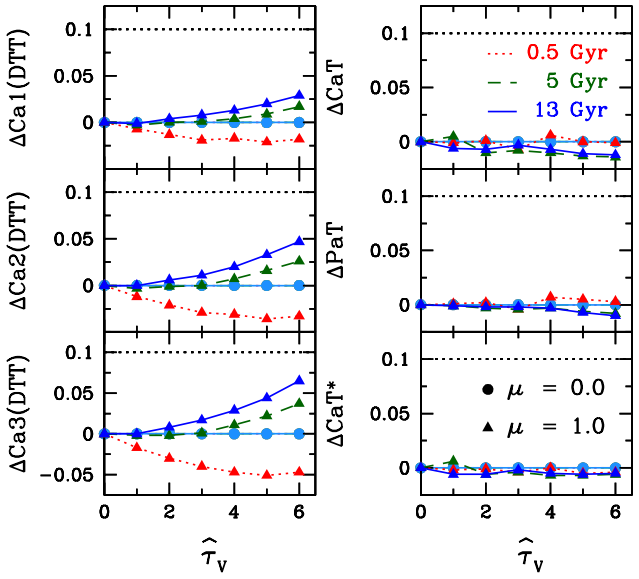

FIG. 8.— Calcium triplet index differences, $\Delta index \equiv index(\hat{\tau}_V) - index(\hat{\tau}_V = 0)$, as a function of $\hat{\tau}_V$ for solar metallicity SSPs. Different ages are represented by: 0.5 (dotted lines; red shades), 5 (dashed lines; green shades), & 13 Gyr (solid lines; blue shades). Different values of μ are represented as 0.0 (circles), and 1.0 (triangles). The black horizontal dotted lines represent typical measurement errors for the different indices.

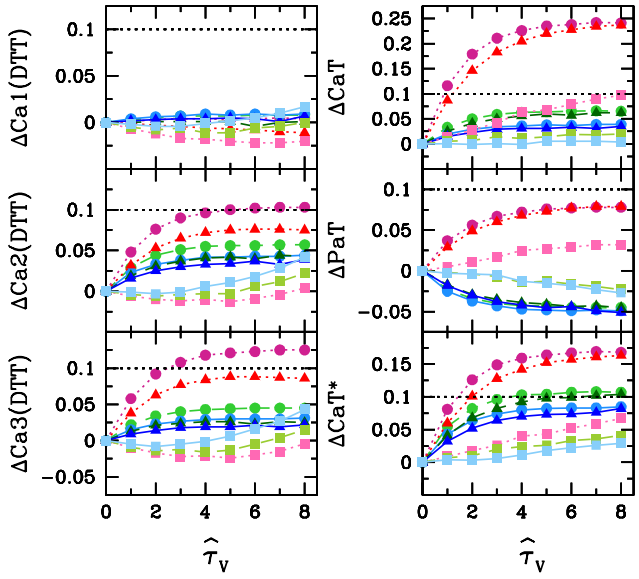

FIG. 9.— Same as Figure 8 but for for an exponential SFH with $\tau_{exp} = 13$ Gyr. Different values of μ are represented by 0.0 (circles), 0.3 (triangles), and 0.9 (squares).

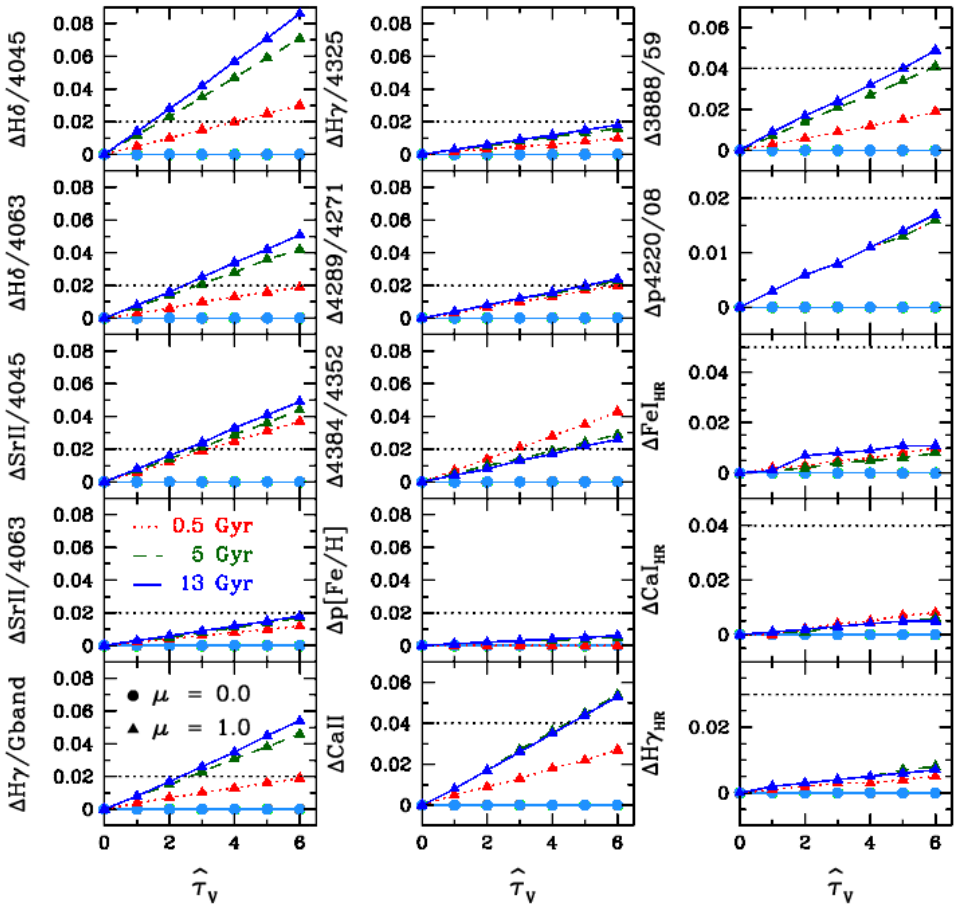

FIG. 10.— Rose index differences, $\Delta index \equiv index(\hat{\tau}_V) - index(\hat{\tau}_V = 0)$, as a function of $\hat{\tau}_V$ for solar metallicity SSPs. Different ages are represented by: 0.5 (dotted lines; red shades), 5 (dashed lines; green shades), & 13 Gyr (solid lines; blue shades). Different values of μ are represented by 0.0 (circles), and 1.0 (triangles). The black horizontal dotted lines represent typical measurement errors for the different indices.

licity errors for a selected number of index–index diagnostic plots are provided in Appendix A. The primary result from this analysis is that, in general, when dust extinction affects the SSP age and metallicity determinations, the errors on the physical parameters are of the same order as the 1σ confidence intervals from typical measurement errors, and thus would not likely be detected above the noise. The most notable exception is any index–index plane using the $D_n(4000)$, which suffers significant errors even in the SSP models. Index–index grids using the longest baseline indices can also suffer significant errors on the measured physical parameters due to the effects of dust.

Figure 13 illustrates the potential pitfalls of discounting dust extinction in an analysis that uses index diagnostics to determine SFHs. There, we plot $H\delta_A$ versus $D_n(4000)$ for the dust-free SSP (gray curves) and exponential SFH (purple curves) models for solar and $Z = 0.05$ metallicity and ages up to 20 Gyr. The triangles represent the $\mu = 0.3$ model indices for $\hat{\tau}_V = 0$ (largest point size and darkest shade) to $\hat{\tau}_V = 8$ (smallest point size, lightest shade). The locus of galaxies in the $H\delta_A$ – $D_n(4000)$ plane has been used to determine their SFHs (e.g. Kauffmann et al. 2003a). Clearly, if a galaxy contains a significant amount of dust, its location in this plane will be best fit by a SFH that is different from its true SFH. As shown, the exponential SFHs move closer to the SSP region when dust is added.

Fortunately, in the Rose dwarf/giant diagnostic plot (Sr II λ4077/Fe Iλ4063 versus Hδ/λ4063), the dust effects run along the lines of constant surface gravity. Thus, this diagnostic plot is still useful for determening the relative amounts of young versus evolved stars, even when dust is present.

It must be emphasized that our analysis has not accounted for emission-line contamination. Dust effects aside, this could potentially be the most worrisome pollutant for all age determinations involving Balmer lines, particularly for the youngest stellar populations. While considering the higher-order Balmer lines (Hγ and Hδ) greatly reduces the problem, it does not go away altogether.

To summarize, we have considered dust effects on absorption-line indices using the Bruzual & Charlot (2003) population synthesis models incorporating the multi-component model of CF00 for the line and continuum attenuation due to dust. For quiescent stellar populations (e.g. spheroids and globular clusters), dust extinction effects are small for most indices. A notable exception is the 4000 Å break, whose sensitivity to dust

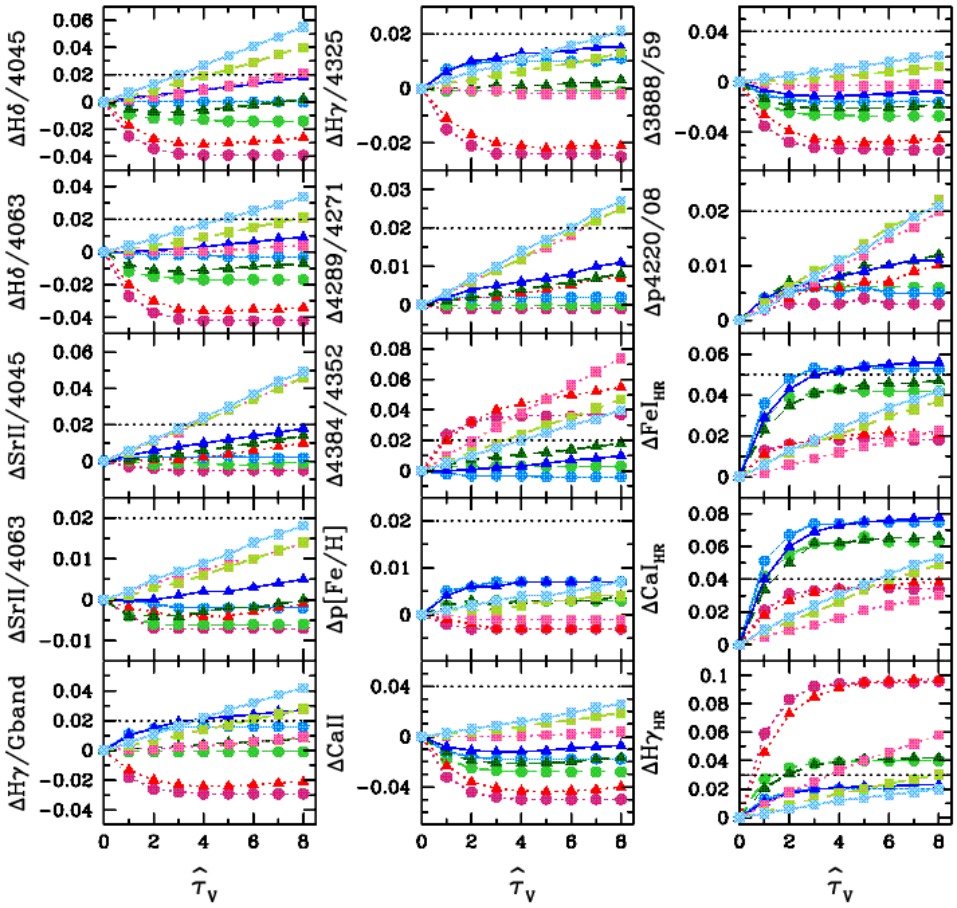

FIG. 11.— Same as Figure 10 but for an exponential SFH with $\tau_{exp} = 13$ Gyr. Different values of μ are represented by 0.0 (circles), 0.3 (triangles), and 0.9 (squares).

can translate into significant errors in the age determination of the stellar population. For models with current SF, many of the indices are significantly modified due to dust reddening effects, and their behavior depends on age, dust distribution, and the effective optical depth. Unfortunately, no simple dust-correction can be prescribed, but future spectroscopic studies of stellar populations in dusty environments (e.g. late-type spirals) ought to consider possible effects due to dust attenuation in their measurements and its resulting effect on physical interpretations. Fortunately, there are particular indices that are negligibly affected by dust extinction (compared to the current level of measurement precision) at different regions in the physical parameter space, and the safest current approach consists of mapping a broad range of indices with the shortest wavelength baselines.

I am most grateful to Stéphane Courteau for his continued advice and support. Special thanks go out to Jim Rose, Ricardo Schiavon, Scott Trager, and Guy Worthey for their careful readings of an early version of the manuscript, and to Jesús González for useful discussions. I would also like to thank the anonymous referee for a detailed report that helped improve this paper. The author acknowledges financial support from the National Science and Engineering Council of Canada.

REFERENCES

Anders, P., Bissantz, N., Fritze-v. Alvensleben, U., de Grijs, R. 2004, MNRAS, 347, 196
Armandroff, T. E. & Zinn, R. 1988, AJ, 96, 92
Balogh, M. L., Morris, S. L., Yee, H. K. C., Carlberg, R. G., & Ellingson, E. 1999, ApJ, 527, 54
Bell, E. F. & de Jong, R. S. 2000, MNRAS, 312, 497
Bergmann, M. P., Jørgensen, I., & Hill G. J. 2003, AJ, 125, 116
Bertelli, G., Bressan,A., Chiosi, C., Fagotto, F., & Nasi, E. 1994, A&AS, 106, 275
Blakeslee, J. P., Vazdekis, A., & Ajhar, E. A. 2001, MNRAS, 320, 193
Bruzual, A. G. 1983, ApJ, 273, 105
Bruzual, A. G. & Charlot, S. 1993, ApJ, 405, 538
Bruzual, A. G. & Charlot, S. 2003, MNRAS, 344, 1000 (GALAXEV)
Bruzual A., G., Magris, G., & Calvet, N. 1988, ApJ, 333, 673
Byun, Y. I., Freeman, K. C., & Kylafis, N. D. 1994, ApJ, 432, 114
Caldwell, N., Rose, J. A., & Concannon, K. D. 2003 AJ, 125, 2891
Cardiel, N., Gorgas, J., Cenarro, J., & González, J. J. 1998, A&AS, 127, 597
Cenarro, A. J., Cardiel, N., Gorgas, J., Peletier, R. F., Vazdekis, A., & Prada, F. 2001a, MNRAS, 326, 959
Cenarro, A. J., Gorgas, J., Cardiel, N., Pedraz, S., Peletier, R. F., & Vazdekis, A. 2001b, MNRAS, 326, 981
Chabrier, G. 2003, PASP, 115, 763
Charlot, S. & Fall, S. M. 2000, ApJ, 539, 718 (CF00)

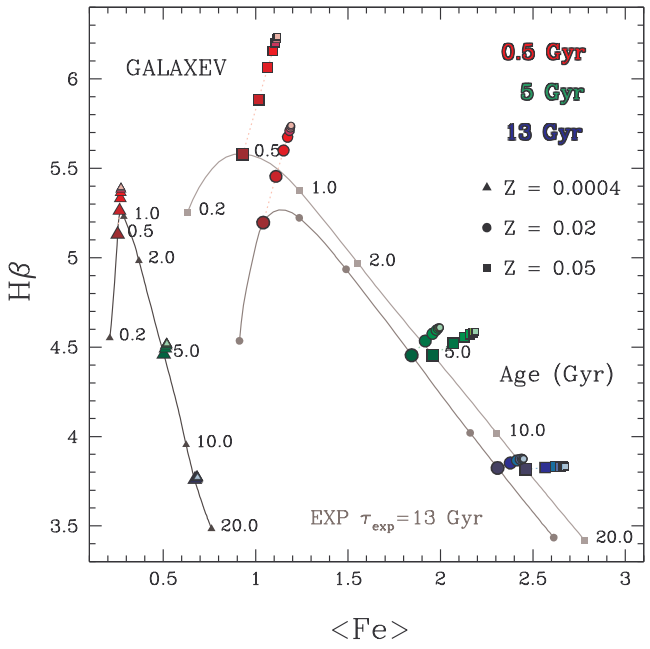

FIG. 12.— Hβ versus $\langle$Fe$\rangle$ for dust-free exponential SFH models with τ_{exp} = 13 Gyr and μ = 0.3 for three metallicities (gray curves), Z = 0.0004 (triangles), 0.02 (circles), and 0.05 (squares). Ages are labeled along the model tracks at 0.2, 0.5, 1.0, 2.0, 5.0, 10.0, and 20.0 Gyr. The colored points (red, green, and blue shades for 0.5, 5, and 13 Gyr respectively) are the model indices measured for the same exponential SFH models, but with dust extinctions from $\hat{\tau}_V = 0$ (largest point size) to $\hat{\tau}_V = 8$ (smallest point size).

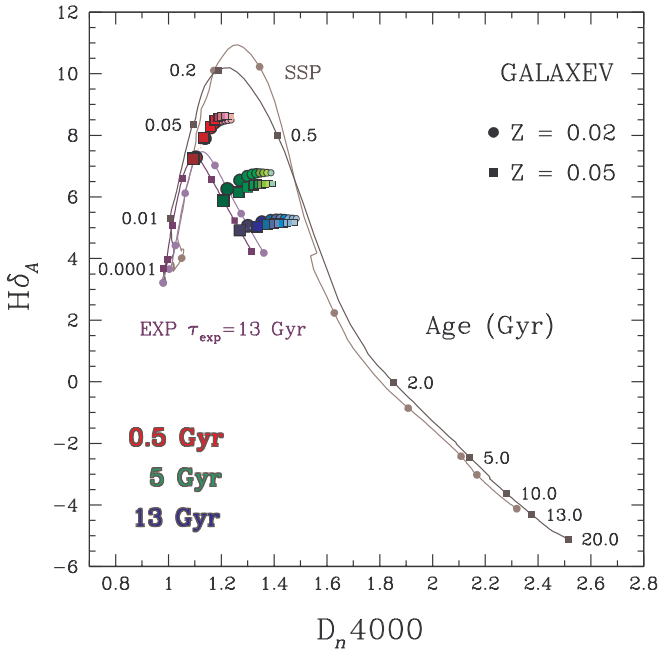

FIG. 13.— Hδ_A versus D$_n$(4000) for dust-free SSPs of solar (circles) and Z=0.05 (squares) metallicity (gray curves) and an exponential SFH with τ_{exp} = 13 Gyr for the same two metallicities (purple curves). Ages are labeled along the model tracks at 0.0001, 0.01, 0.05, 0.2, 0.5, 1.0, 2.0, 5.0, 10.0, 13.0, and 20.0 Gyr. The colored points (red, green, and blue shades for 0.5, 5, and 13 Gyr respectively) are the model indices measured for exponential SFH models of the same two metallicities, but with dust extinctions from $\hat{\tau}_V = 0$ (largest point size) to $\hat{\tau}_V = 8$ (smallest point size).

Charlot, S., Worthey, G. & Bressan, A. 1996, ApJ, 457, 625
Charlot, S., Kauffmann, G., Longhetti, M., Tresse, L., White, S. D. M., Maddox, S. J., & Fall, S. M. 2002, MNRAS, 330, 876
de Jong, R. S. 1996, A&A, 313, 377
Delisle, S. & Hardy, E. 1992, AJ, 103, 711
Diaz, A. I., Terlevich, E., & Terlevich, R. 1989, MNRAS, 239, 325 (DTT)
de Jong, R. S. 1996, A&A, 313, 377
de Zeeuw, P. T. et al. 2002, MNRAS, 329, 513
Falcón-Barroso, J. Peletier, R. F., Vazdekis, A., & Balcells, M. 2003 ApJ, 588, L17
Ferland, G. J. 2002, Hazy, a brief introduction to CLOUDY (University of Kentucky, Dept. of Physics & Astronomy Int. Rep.)
Fioc, M. & Rocca-Volmerange, B. 1997, A&A, 326, 950
Fisher, D., Franx, M., & Illingworth, G. 1996, ApJ, 459, 110
González, J. J. 1993, Ph.D. thesis, Univ. California, Santa Cruz
Gordon, K. D., Misselt, K. A., Witt, A. N., & Clayton, G. C. 2001, ApJ, 551, 269
Gorgas, J., Faber, S. M., Burstein, D., González, J. J., Courteau, S., & Prosser, C. 1993, ApJS, 86, 153
Gorgas, J., Cardiel, N., Pedraz, S. & González, J. J. 1999, 139, 29
Goudfrooij, P., Gorgas, J., & Jablonka, P. 1999, Ap&SS, 269, 109
Jones, J. E., Alloin, D. M., & Jones, B. J. T. 1984, ApJ, 283, 457
Jones, L. A. & Worthey, G. 1995, ApJ, 446, L31
Kauffmann, G., et al. 2003a, MNRAS, 341, 33
Kauffmann, G., et al. 2003b, MNRAS, 341, 54
Leonardi, A. J. & Worthey, G 2000 ApJ, 534, L650
Liu, M. C., Charlot, S., & Graham, J. R. 2000, ApJ, 543, 644
Loveday J., Peterson B. A., Maddox S. J., & Efstathiou G., 1996, ApJS, 107, 201
MacArthur, L. A., Courteau, S., Bell, E., & Holtzman, J. A. 2004, ApJS, 152, 175
Maraston, C. 1998, MNRAS, 300, 872
Maraston, C. & Thomas, D. 2000, ApJ, 541, 126
Moy, E., Rocca-Volmerange, B., & Fioc, M. 2001, A&A, 365, 347
Osterbrock, D. E. 1989, Astrophysics of Gaseous Nebulae and Active Galactic Nuclei (Mill Valley: University Science)
Panuzzo, P., Bressan, A., Granato, G. L., Silva, L., & Danese, L. 2003, A&A, 409, 99
Proctor, R. N. & Sansom, A. E. 2002, MNRAS, 333, 517
Rose, J .A. 1984 AJ, 89, 1238
Rose, J .A. 1985 AJ, 90, 1927
Rose, J .A. 1994 AJ, 107, 206
Schiavon, R. P., Faber, S. M., Rose, J. A., & Castilho, B. V. 2002, ApJ, 580, 873
Silva, L., Granato, G. L., Bressan, A. & Danese, L. 1998, ApJ, 509, 103
Tantalo, R. & Chiosi, C. 2004, MNRAS accepted, astro-ph/0305247
Thomas, D., Maraston, C., & Bender, R. 2003, MNRAS, 339, 897
Tinsley, B. M. 1972, ApJ, 178, 319
Trager, S. C., Worthey, G., Faber, S. M., Burstein, D., & Gonzalez, J. J. 1998, ApJS, 116, 1
Trager, S. C., Dalcanton, J. J., & Weiner, B. J. 1999, The Formation of Galactic Bulges, 42
Trager, S. C., Faber, S. M., Worthey, G., & González, J. J. 2000, AJ, 119, 1645
Vazdekis, A. 1999, ApJ, 513, 224
Vazdekis, A. & Arimoto, N. 1999, ApJ, 525, 144
Vazdekis, A., Salaris, M., Arimoto, N., & Rose, J. A. 2001, ApJ, 549, 274
Vazdekis, A., Cenarro, A. J., Gorgas, J., Cardiel, N., & Peletier, R. F. 2003, MNRAS, 340, 1317
Witt, A. N., Thronson, H. A., & Capuano, J. M. 1992, ApJ, 393, 611
Worthey, G. 1993, ApJ, 409, 530
Worthey, G. 1994, ApJS, 95, 107
Worthey, G., Faber, S. M., Gonzalez, J. J., & Burstein, D. 1994, ApJS, 94, 687
Worthey, G. & Ottaviani, D. L. 1997, ApJS, 111, 377 (WO97)

APPENDIX

AGE AND METALLICITY FITTING

In order to translate absorption-line indices to a physical age and metallicity scale, the index measurements must be compared with stellar population synthesis models. In their most basic form, commonly referred to as simple stellar populations (SSPs), these models provide evolutionary information for a coeval population of stars born with a given composition and initial mass function (IMF). Several such SSP models have been produced by a number of independent groups and are in a constant state of flux as improvements to many of the input parameters (e.g. stellar libraries, model atmospheres, convection, mass loss, mixing) come to light. There are discrepancies among the different models that, depending on the application, may result in significantly different interpretations of the observed stellar population signatures. We are not interested here in a detailed comparison of the different SPS models, but rather seek a quantitative guide for the magnitude of the errors due to dust effects on the physical parameters derived from absorption-line indices. To this end, we use the 2003 implementation of the Bruzual & Charlot (2003) SPS models (GALAEX) for the age and metallicity determinations, the same as are used to compute the model "galaxies" (see §3).

While most galaxies have likely undergone SFHs that are much more complex than the simple SSP described above, the common practice for line-index measurements is to compute "SSP-ages and metallicities", that is, compare the galaxy indices to the SSP grids, irrespective of the true SFH of the galaxy (which is unknown). We adopt this technique here and thus refer to SSP parameters even for the models with exponential SFHs.

Ages and metallicities are determined by fitting the model galaxy index measurements to the SSP model grids using a maximum-likelihood approach. We retain the same grid in time as is provided in the model SSPs (220 unequally spaced time steps from t = 0–20 Gyr) and interpolate (linearly) between the model metallicities on a fine grid of 120 unequally spaced steps in Z. In order to compare all indices on a similar scale, the atomic indices computed as equivalent widths in Å, I_{EW}, are converted to a magnitude, I_{mag}, as:

$$I_{mag} = -2.5 \log_{10}\left(1 - \frac{I_{EW}}{\Delta\lambda}\right) \tag{A1}$$

where $\Delta\lambda$ is the width in Å of the index feature bandpass. The corresponding error in magnitude is:

$$\sigma_{mag} = \frac{2.5 \log_{10}(e)}{\Delta\lambda\, 10^{-0.4 I_{mag}}}\, \sigma_{EW}. \tag{A2}$$

The two definitions of the 4000 Å break, which are dimensionless flux ratios, are converted to a magnitude scale as:

$$\mathrm{D4000}_{mag} = -2.5 \log_{10}\left(\mathrm{D4000}_{ratio}\right) \tag{A3}$$

with the corresponding error in magnitude as:

$$\sigma[\mathrm{D4000}_{mag}] = 2.5 \log_{10}(e) \frac{\sigma[\mathrm{D4000}_{ratio}]}{\mathrm{D4000}_{ratio}}. \tag{A4}$$

We compute an age and metallicity by minimizing the following figure of merit:

$$FOM = \frac{1}{N-1} \sum_{i=1}^{N} \frac{[O_i - M(A,Z)_i]^2}{\delta O_i^2}, \tag{A5}$$

where N is the number of indices (only 2 are used here, but this method could be generalized to fit multiple indices simultaneously), O_i is the "observed" value (in magnitudes) of index i and δO_i is its error in magnitudes, and $M(A,Z)_i$ is the SSP model value of index i for a given age and metallicity combination.

Errors for the individual age and metallicity measurements are estimated using a Monte Carlo approach. One thousand realizations of the model fits are computed using errors drawn from a normal distribution of the observational errors (taken here as the "typical" observation errors for each index quoted in §4.1). The errors for the measured ages and metallicities are taken as half the interval containing 68% of the 1000 Monte Carlo realizations (i.e. the 1σ confidence interval). Two examples of the fits are given in Figure A14 which shows the logarithmic difference between the physical parameters derived from each simulated point relative to the best-fit value for the $D_n(4000)$ – Fe4668 plane (see also the corresponding index–index plot in Figure A15 [right panel]). The left panel presents the fit for the dust-free ($\mu = 0.0$) SSP case which indeed finds the correct model age (A = 5 Gyr; $\Delta \log_{10}$[Age (Gyr)] = 0) and metallicity (Z = 0.02; $\Delta[\log_{10}(Z/Z_\odot)] = 0$), with corresponding 1σ confidence intervals (represented as error bars) of ~ 0.2 dex for both parameters. The right panel presents the fit for the dusty case ($\mu = 1.0$) at 0.5 Gyr (but note the different y-axis scales). The $\hat{\tau}_V = 0$ fit finds the correct physical parameters, but as the dust opacity increases, the best fit wanders around in age (from A = 0.5 Gyr at $\hat{\tau}_V = 0$ to A = 10.0 Gyr at $\hat{\tau}_V = 6$) and metallicity (from Z = 0.02 at $\hat{\tau}_V = 0$ to $Z = 0.003$ at $\hat{\tau}_V = 6$). Since we do not consider extrapolations, there are "edges" in these plots that represent the limits of the model grids. As a result, the confidence limits can be underestimated for points fit near the model grid limits, which also generally correspond to a region of greater degeneracy in age and metallicity. As a result, any points that lie near the model limits should be treated with caution.

Given that we are comparing model galaxies with exponential SFHs against SSP grids, it is inevitable that some of the parameter space will fall outside the model grids and thus cannot be fit reliably. In fact, even for some of the SSP models, the dust extinction can be severe enough to push the locus of the model point in the index–index diagram off the SSP model grids. Both of these situations are observed in the $D_n(4000)$ versus Fe4668 index–index diagram in Figure A15 [right panel].

Tables 1 & 2 present the results from our age and metallicity fitting for a selected number of index–index combinations: Hβ versus Mgb, Mg_2, and [MgFe]$'$ (top) and Hβ, Hδ_A, and $D_n(4000)$ versus Fe4668 (bottom) for the SSP and exponential SFH model galaxies respectively (tables for other index combinations are available from the author upon request). For each index-pair, we list the model age, MA, the effective V-band optical depth, $\hat{\tau}_V$, whether the fit is reliable in the "fit" column (see below), the best-fit age with its 1σ error in brackets, the difference between the measured age in the extincted models and the dust-free age, $\Delta\mathrm{A} \equiv \mathrm{Age}(\hat{\tau}_V) - \mathrm{Age}(\hat{\tau}_V = 0)$, and the same for the metallicities, which are given as $\log_{10}(Z/Z_\odot)$ and $\Delta Z \equiv \log_{10}(Z/Z_\odot)(\hat{\tau}_V) - \log_{10}(Z/Z_\odot)(\hat{\tau}_V = 0)$. Reliable fits are indicated with a check mark, ✓. For unreliable fits the check mark is replaced with a code indicating the reason for which they could not be fit. The codes are: "OG" if the point lies off the model grids, "DB" if it lies in the young double-valued Balmer line region, and "DM" if it lies in a degenerate metallicity region (only occurred for the young exponential SFH model in the $D_n(4000)$ – Fe4668 plane). Note that, in the absence of a reliable fit for the dust-free case, even if reliable fits exist for the corresponding dusty models, the Δ's are not well defined (only occurred for the 0.5 Gyr exponential SFH model in Table 2 in the $D_n(4000)$ – Fe4668 plane). Examples of the messy double-valued Balmer line region can be seen in the Hβ versus Mgb plot in Figure A15 [left panel] where the ages plotted extend down to 0.002 Gyr, as well as in Figures 12 & 13 in §5.

It is obvious from Tables 1 & 2 (and see Fig. A14) that there is significant uncertainty in the fits given our assumed "typical" measurement errors, regardless of the dust content. For example, the 0.5 Gyr SSP model 1σ confidence limits (Table 1) range from ∼0.1–0.4 Gyr in age and ∼0.2–0.3 dex in metallicity, depending on the index–index grid used. Note that the 1σ confidence limits are not only dependent on the particular index-index plane used, but they also depend on the location of the point within the grid (in other words, to what degree the age and metallicity are separated at the given locus). In general, the degeneracies become more severe at the extreme metallicities (i.e. $Z \lesssim 0.001$ and $Z \gtrsim 0.02$), and at young ages, where both the narrower region covered by the metallicity span and the double-valued Balmer lines contribute to the problem.

As expected from §4, the fits for the 0.5 Gyr SSP models (Table 1) are virtually unaffected by dust (for the index–index planes shown), with the exception of the $D_n(4000)$ – Fe4668 plane, for which the age and metallicity errors are large (up to 9.5 Gyr and 0.8 dex respectively) and significant compared to the 1σ confidence limits, even for small amounts of dust. Significant errors occur at the highest dust opacities for the 5 Gyr models (in all but the Hβ – Mgb and [MgFe]$'$ planes), but in this case they are of the same order as the 1σ confidence limits. The errors due to dust on age and metallicity are most severe in the 13 Gyr models, with some points ending up off the model grids at the highest $\hat{\tau}_V$'s (e.g. in the Hβ and Hδ_A versus Fe4668 grids), but these are again matched by the large 1σ confidence limits for fits in these regions of the grid. In summary, for the SSP model galaxies, if the model indices lie in a region of the index–index diagnostic plot where the age and metallicity are well separated (close to orthogonal), the fits are generally independant of dust extinction for most index combinations. Where the fits are affected by the dust (generally at older ages and for indices with broader baselines), the errors in the derived ages and metallicities are generally of the same order as the 1σ confidence limits and would thus be difficult to detect. The most notable exceptions here are the Hβ–Mg_2 plane, where the dust pushes the points for the 0.5 Gyr models into the degenerate double-valued Balmer line region, and the $D_n(4000)$ – Fe4668 plane, where the errors due to dust become large at young ages, and at old ages the points extend off the edges of the model grids.

On the other hand, for the exponential SFH models, again as expected from §4, the situation is more complicated. Examination of Table 2 reveals that none of the 0.5 Gyr models can be fit reliably in the Balmer-index versus metallicity-index grids as they all fall in the double-valued Balmer line region of the plots. Reliable fits for the dustier 0.5 Gyr models in the $D_n(4000)$ – Fe4668 plane are obtained, but here the Δ's are undefined due to the poor fit in the dust-free model. Reliable fits are found for most of the 5 Gyr exponential SFH models with "SSP ages" in the range ∼0.9–1.0 Gyr (i.e. this is the luminosity-weighted SSP age of a 5 Gyr old stellar population that has been forming stars at a constant rate, roughly, throughout its lifetime). The ages, when reliably fit, generally agree between the different index–index plane fits. When dust has an effect on the ages, it tends to make them slightly youger, but the ΔA's are always of the same order as the 1σ confidence limits for the fits. The metallicity fits for these models, which are all inherently solar metallicity, are in the range $\log_{10}(Z/Z_\odot) \sim -0.7$ to $+0.2$ (or $Z = 0.004$ – 0.03). They are generally lower(higher) than solar in the 5 (13) Gyr models and increase with dust extinction. Unlike the age fits, the metallicity fits do not agree very well between the different index–index planes. For example, the $\hat{\tau}_V = 0$ fit in 13 Gyr models gives $\log_{10}(Z/Z_\odot) = +0.32$ and -0.12 dex in the Hβ – Mgb and Hβ – Fe4668 planes respectively. The ages for the 13 Gyr exponential SFH model fits are also in the ∼0.9–1.0 Gyr range. While these do have weaker Balmer lines than the 5 Gyr models, their metallicity index values are slightly stronger. This has the overall effect of moving them along a line of roughly constant age. An example of this is shown by the 5 Gyr (green) and 13 Gyr (blue) triangles in the Hβ versus Mgb diagnostic plot in Figure A15 [left panel]. These results highlight once again the greater challenge of fitting reliable ages and metallicities for "young" populations.

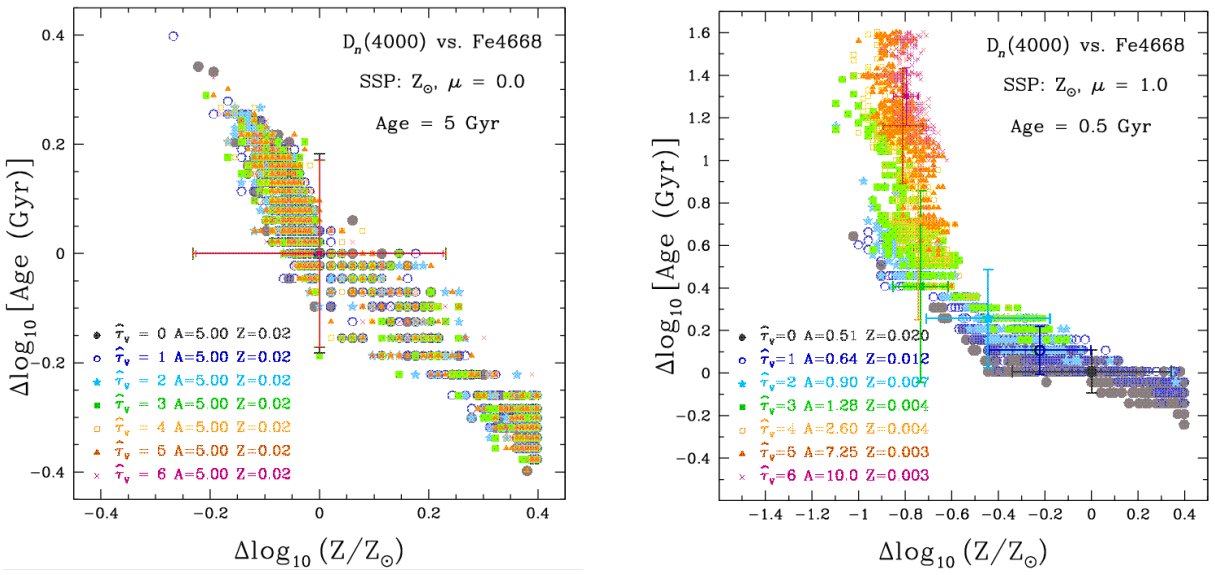

FIG. A14.— Examples of the Monte Carlo fits for D$_n$(4000) versus Fe4668 diagnostic plots, represented as the logarithmic difference between the physical parameter derived from each simulated point relative to the best-fit value (also see the corresponding index–index plot in Figure A15, right panel). The error bars represent the 1σ confidence limits. Left: SSP model at 5 Gyr with $\mu = 0.0$. Right: SSP model at 0.5 Gyr with $\mu = 1.0$ (note the different y-axis scales).

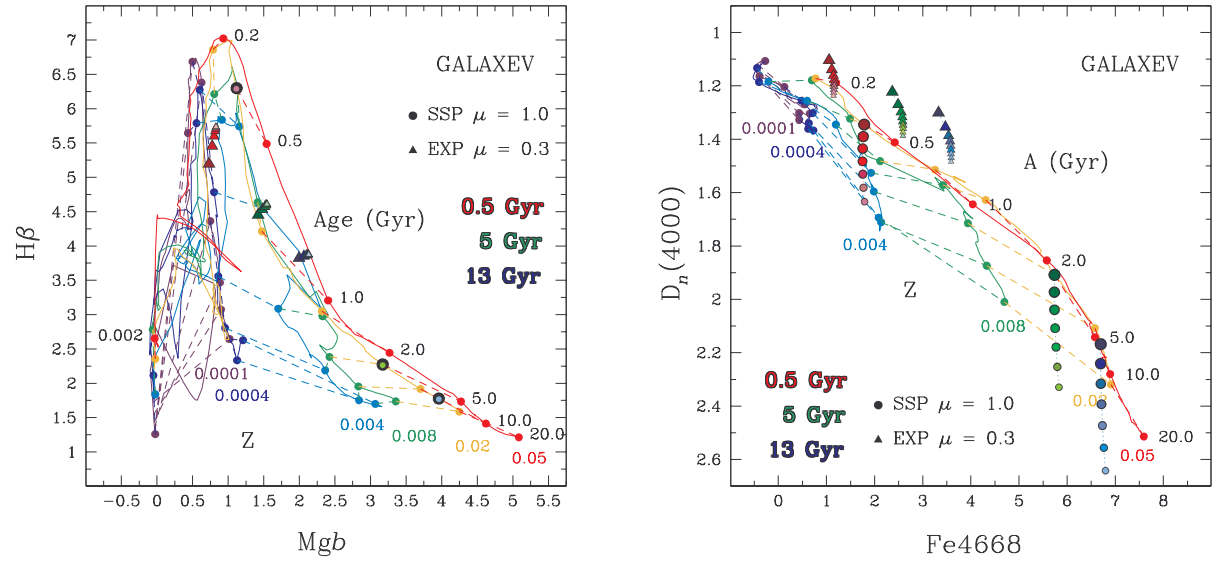

FIG. A15.— Hβ versus Mgb [left] and D$_n$(4000) versus Fe4668 [right] diagnostic plots. The grids are dust-free BC03 SSP models. Lines of constant age (dashed) are shown for ages 0.2, 0.5, 1.0, 2.0, 5.0, 10.0, and 20.0 Gyr in both panels, but in the Hβ versus Mgb plot (left), the age extends to 0.002 Gyr to illustrate the messy young age, double-valued Balmer line, region (see text). Lines of constant metallicity (solid) are shown for Z = 0.0001 (purple), 0.0004 (dark blue), 0.004 (light blue), 0.008 (green), 0.02 (yellow), and 0.05 (red). The circles are the indices measured from the solar metallicity SSP models with $\mu = 1.0$ for $\hat{\tau}_V = 0$ (largest point size) to $\hat{\tau}_V = 6$ (smallest point size), and the triangles are the exponential SFH model indices with $\tau_{exp} = 13$ Gyr and $\mu = 0.3$ for $\hat{\tau}_V = 0$ (largest point size) to $\hat{\tau}_V = 8$ (smallest point size). The red, green, and blue shades are for model ages of 0.5, 5, and 13 Gyr respectively.

TABLE 1
AGE & METALLICITY FITS AND ERRORS: SSP WITH $Z = Z_\odot$ AND $\mu = 1.0$.

		Hβ vs. Mgb					Hβ vs. Mg$_2$					Hβ vs. [MgFe]$'$				
MA	$\hat{\tau}_V$	fit[a]	Age	ΔA	log($Z/Z_\odot$)	ΔZ	fit[a]	Age	ΔA	log($Z/Z_\odot$)	ΔZ	fit[a]	Age	ΔA	log($Z/Z_\odot$)	ΔZ
0.5	0	✓	0.51 (0.22)	0.00	0.00 (0.35)	0.00	DB	0.51 (0.43)	0.00	0.00 (0.38)	0.00	✓	0.51 (0.10)	0.00	0.00 (0.33)	0.00
	2	✓	0.51 (0.22)	0.00	0.00 (0.36)	0.00	DB	0.45 (0.36)	-0.06	-0.44 (0.74)	-0.44	✓	0.51 (0.10)	0.00	-0.01 (0.33)	-0.01
	4	✓	0.51 (0.22)	0.00	0.00 (0.36)	0.00	DB	0.45 (0.36)	-0.06	-0.46 (0.77)	-0.46	✓	0.51 (0.10)	0.00	-0.01 (0.32)	-0.01
	6	✓	0.51 (0.22)	0.00	0.00 (0.35)	0.00	DB	0.09 (0.19)	-0.42	0.29 (0.38)	0.29	✓	0.51 (0.10)	0.00	0.00 (0.34)	0.00
5	0	✓	5.00 (1.63)	0.00	0.00 (0.13)	0.00	✓	5.00 (1.50)	0.00	0.00 (0.09)	0.00	✓	5.00 (1.63)	0.00	0.00 (0.13)	0.00
	2	✓	5.00 (1.50)	0.00	0.00 (0.12)	0.00	✓	5.00 (1.50)	0.00	0.00 (0.09)	0.00	✓	5.00 (1.50)	0.00	0.00 (0.12)	0.00
	4	✓	5.00 (1.50)	0.00	0.00 (0.12)	0.00	✓	4.50 (1.63)	-0.50	0.06 (0.13)	0.06	✓	5.00 (1.75)	0.00	0.00 (0.14)	0.00
	6	✓	5.00 (1.50)	0.00	0.00 (0.12)	0.00	✓	4.25 (1.57)	-0.75	0.11 (0.18)	0.11	✓	4.75 (1.75)	-0.25	0.04 (0.14)	0.04
13	0	✓	13.00 (6.25)	0.00	0.00 (0.21)	0.00	✓	13.00 (4.38)	0.00	0.00 (0.13)	0.00	✓	13.00 (5.88)	0.00	0.00 (0.22)	0.00
	2	✓	11.50 (6.00)	-1.50	0.08 (0.20)	0.08	✓	13.25 (4.38)	0.25	0.00 (0.13)	0.00	✓	12.25 (6.00)	-0.75	0.04 (0.22)	0.04
	4	✓	10.50 (6.25)	-2.50	0.13 (0.21)	0.13	✓	11.50 (4.75)	-1.50	0.08 (0.13)	0.08	✓	11.25 (6.00)	-1.75	0.10 (0.22)	0.10
	6	✓	10.50 (5.87)	-2.50	0.13 (0.20)	0.13	✓	9.50 (4.75)	-3.50	0.19 (0.15)	0.19	✓	10.00 (6.00)	-3.00	0.16 (0.22)	0.16
		Hβ vs. Fe4668					Hδ_A vs. Fe4668					D$_n$(4000) vs. Fe4668				
0.5	0	✓	0.51 (0.10)	0.00	0.00 (0.31)	0.00	✓	0.51 (0.10)	0.00	0.00 (0.18)	0.00	✓	0.51 (0.12)	0.00	0.00 (0.34)	0.00
	2	✓	0.51 (0.10)	0.00	-0.03 (0.34)	-0.03	✓	0.51 (0.15)	0.00	-0.02 (0.15)	-0.02	✓	0.90 (0.48)	0.40	-0.44 (0.27)	-0.44
	4	✓	0.51 (0.10)	0.00	-0.03 (0.34)	-0.03	✓	0.51 (0.10)	0.00	-0.02 (0.16)	-0.02	✓	2.60 (2.80)	2.09	-0.74 (0.10)	-0.74
	6	✓	0.51 (0.10)	0.00	0.00 (0.31)	0.00	✓	0.51 (0.06)	0.00	0.00 (0.09)	0.00	✓	10.00 (3.13)	9.49	-0.80 (0.05)	-0.80
5	0	✓	5.00 (1.93)	0.00	0.00 (0.22)	0.00	✓	5.00 (2.33)	0.00	0.00 (0.22)	0.00	✓	5.00 (2.03)	0.00	0.00 (0.23)	0.00
	2	✓	5.00 (1.80)	0.00	0.00 (0.22)	0.00	✓	5.00 (2.38)	0.00	0.00 (0.23)	0.00	✓	11.00 (2.12)	6.00	-0.12 (0.05)	-0.12
	4	✓	3.50 (1.93)	-1.50	0.18 (0.22)	0.18	✓	4.00 (2.05)	-1.00	0.15 (0.23)	0.15	OG	20.00 (2.00)	15.00	-0.15 (0.02)	-0.15
	6	✓	3.00 (1.80)	-2.00	0.29 (0.22)	0.29	✓	3.25 (1.93)	-1.75	0.24 (0.22)	0.24	OG	20.00 (0.00)	15.00	-0.07 (0.02)	-0.07
13	0	✓	13.00 (3.00)	0.00	0.00 (0.12)	0.00	✓	13.00 (4.00)	0.00	0.00 (0.20)	0.00	✓	13.00 (2.50)	0.00	0.00 (0.11)	0.00
	2	✓	12.75 (3.12)	-0.25	0.02 (0.11)	0.02	✓	12.75 (4.13)	-0.25	0.02 (0.21)	0.02	OG	20.00 (1.50)	7.00	-0.02 (0.04)	-0.02
	4	OG	12.00 (3.12)	-1.00	0.06 (0.10)	0.06	✓	6.25 (8.25)	-6.75	0.39 (0.42)	0.39	OG	17.00 (0.00)	4.00	0.37 (0.03)	0.37
	6	OG	12.25 (2.87)	-0.75	0.06 (0.09)	0.06	OG	7.50 (3.38)	-5.50	0.37 (0.21)	0.37	OG	20.00 (0.00)	7.00	0.40 (0.00)	0.40

NOTE. — All ages are given in Gyr and metallicities as $\log_{10}(Z/Z_\odot)$. The numbers in brackets next to the age and metallicity measurements are the 1σ confidence limits on the derived values based on 1000 Monte Carlo realizations drawn from a Gaussian distribution of the measurement errors.

[a]A check mark, ✓, indicates a reliable fit. Unreliable fits are coded as: "OG" if the point lies off the model grids, and "DB" if it lies in the young double-valued Balmer line region.

TABLE 2
AGE & METALLICITY ERRORS: EXPONENTIAL SFH WITH $\tau_{exp} = 13$ GYR AND $\mu = 0.3$.

		Hβ vs. Mgb					Hβ vs. Mg$_2$					Hβ vs. [MgFe]$'$				
MA	$\hat{\tau}_V$	fit[a]	Age	ΔA	log($Z/Z_\odot$)	ΔZ	fit[a]	Age	ΔA	log($Z/Z_\odot$)	ΔZ	fit[a]	Age	ΔA	log($Z/Z_\odot$)	ΔZ
0.5	0	DB	0.08 (0.02)	0.00	-0.49 (0.50)	0.00	DB	0.06 (0.03)	0.00	-0.10 (0.52)	0.00	DB	0.06 (0.33)	0.00	-0.01 (0.43)	0.00
	2	DB	0.11 (0.04)	0.03	-0.60 (0.21)	-0.11	DB	0.64 (0.60)	0.58	-0.60 (0.53)	-0.51	DB	0.64 (0.54)	0.58	-0.82 (0.19)	-0.82
	4	DB	0.14 (0.26)	0.06	-0.62 (0.21)	-0.12	DB	0.08 (0.27)	0.02	0.02 (0.53)	0.12	DB	0.57 (0.19)	0.51	-0.76 (0.10)	-0.75
	6	DB	0.14 (0.26)	0.06	-0.60 (0.22)	-0.11	DB	0.03 (0.54)	-0.03	0.40 (1.08)	0.49	DB	0.57 (0.19)	0.51	-0.76 (0.08)	-0.75
	8	DB	0.14 (0.22)	0.06	-0.60 (0.19)	-0.11	DB	0.09 (0.26)	0.03	-0.05 (0.51)	0.05	DB	0.26 (0.39)	0.20	-0.70 (0.09)	-0.69
5	0	✓	1.02 (0.11)	0.00	-0.18 (0.45)	0.00	✓	0.90 (0.10)	0.00	0.10 (0.19)	0.00	✓	1.02 (0.00)	0.00	-0.22 (0.19)	0.00
	2	✓	1.02 (0.21)	0.00	-0.68 (0.90)	-0.50	✓	0.81 (0.10)	-0.10	0.22 (0.12)	0.12	✓	0.90 (0.11)	-0.11	0.04 (0.22)	0.26
	4	✓	0.81 (0.21)	-0.21	0.20 (0.41)	0.38	✓	0.81 (0.10)	-0.10	0.20 (0.12)	0.11	✓	0.90 (0.10)	-0.11	0.04 (0.22)	0.26
	6	✓	0.81 (0.21)	-0.21	0.20 (0.36)	0.38	✓	0.81 (0.09)	-0.10	0.20 (0.12)	0.11	✓	0.90 (0.10)	-0.11	0.04 (0.21)	0.26
	8	✓	0.81 (0.21)	-0.21	0.20 (0.34)	0.38	✓	0.81 (0.10)	-0.10	0.20 (0.12)	0.11	✓	0.90 (0.10)	-0.11	0.04 (0.22)	0.26
13	0	✓	0.90 (0.11)	0.00	0.32 (0.07)	0.00	✓	0.90 (0.11)	0.00	0.33 (0.08)	0.00	✓	1.02 (0.12)	0.00	0.20 (0.18)	0.00
	2	✓	0.90 (0.10)	0.00	0.33 (0.04)	0.01	✓	0.90 (0.10)	0.00	0.33 (0.04)	0.00	✓	0.90 (0.11)	-0.11	0.32 (0.07)	0.12
	4	✓	0.90 (0.10)	0.00	0.33 (0.04)	0.01	✓	0.90 (0.10)	0.00	0.33 (0.04)	0.00	✓	0.90 (0.10)	-0.11	0.32 (0.07)	0.12
	6	✓	0.90 (0.10)	0.00	0.33 (0.04)	0.01	✓	0.90 (0.10)	0.00	0.33 (0.04)	0.00	✓	0.90 (0.10)	-0.11	0.32 (0.06)	0.12
	8	✓	0.90 (0.10)	0.00	0.33 (0.04)	0.01	✓	0.90 (0.10)	0.00	0.33 (0.04)	0.00	✓	0.90 (0.10)	-0.11	0.32 (0.06)	0.12
		Hβ vs. Fe4668					Hδ_A vs. Fe4668					$D_n(4000)$ vs. Fe4668				
0.5	0	DB	0.04 (0.34)	0.00	0.22 (0.44)	0.00	DB	0.04 (0.98)	0.00	0.28 (0.99)	0.00	DM	0.07 (0.05)	0.00	-0.01 (0.32)	0.00
	2	DB	0.64 (0.58)	0.60	-0.60 (0.72)	-0.82	DB	0.81 (0.42)	0.77	-0.72 (0.76)	-1.00	OG	0.18 (0.11)	0.11	0.40 (0.80)	0.41
	4	DB	0.64 (0.57)	0.60	-0.54 (0.33)	-0.76	DB	0.81 (0.72)	0.77	-0.72 (0.74)	-1.00	✓	0.20 (0.04)	0.13	0.37 (0.32)	0.38
	6	DB	0.64 (0.57)	0.60	-0.54 (0.32)	-0.76	DB	0.81 (0.72)	0.77	-0.72 (0.74)	-1.00	✓	0.26 (0.05)	0.18	0.10 (0.39)	0.11
	8	DB	0.64 (0.57)	0.60	-0.54 (0.32)	-0.76	DB	0.81 (0.72)	0.77	-0.72 (0.72)	-1.00	✓	0.32 (0.07)	0.25	-0.22 (0.34)	-0.21
5	0	✓	1.02 (0.00)	0.00	-0.24 (0.07)	0.00	✓	1.02 (0.12)	0.00	-0.25 (0.14)	0.00	OG	0.32 (0.03)	0.00	0.40 (0.00)	0.00
	2	✓	1.02 (0.11)	0.00	-0.24 (0.12)	0.00	✓	0.90 (0.10)	-0.11	-0.09 (0.16)	0.17	OG	0.45 (0.05)	0.13	0.39 (0.01)	-0.01
	4	✓	1.02 (0.11)	0.00	-0.24 (0.13)	0.00	✓	0.90 (0.15)	-0.11	-0.09 (0.24)	0.17	OG	0.45 (0.05)	0.13	0.40 (0.00)	0.00
	6	✓	1.02 (0.11)	0.00	-0.24 (0.14)	0.00	✓	0.90 (0.15)	-0.11	-0.09 (0.23)	0.17	OG	0.51 (0.06)	0.19	0.38 (0.02)	-0.02
	8	✓	1.02 (0.11)	0.00	-0.24 (0.12)	0.00	✓	0.90 (0.15)	-0.11	-0.09 (0.24)	0.17	OG	0.51 (0.06)	0.19	0.40 (0.05)	0.00
13	0	✓	1.14 (0.12)	0.00	-0.12 (0.20)	0.00	✓	1.02 (0.17)	0.00	0.06 (0.26)	0.00	OG	0.57 (0.07)	0.00	0.40 (0.00)	0.00
	2	✓	1.02 (0.12)	-0.12	0.18 (0.20)	0.30	OG	0.81 (0.33)	-0.21	0.37 (0.22)	0.31	OG	1.02 (0.37)	0.44	0.00 (0.40)	-0.40
	4	✓	1.02 (0.12)	-0.12	0.18 (0.19)	0.30	OG	0.81 (0.33)	-0.21	0.37 (0.21)	0.31	OG	1.02 (0.28)	0.44	0.00 (0.34)	-0.40
	6	✓	1.02 (0.12)	-0.12	0.18 (0.19)	0.30	OG	0.81 (0.33)	-0.21	0.37 (0.21)	0.31	OG	1.02 (0.26)	0.44	0.00 (0.00)	-0.40
	8	✓	1.02 (0.12)	-0.12	0.18 (0.19)	0.30	OG	0.81 (0.33)	-0.21	0.37 (0.21)	0.31	OG	1.28 (0.26)	0.71	0.00 (0.02)	-0.40

NOTE. — All ages are given in Gyr and metallicities as $\log_{10}(Z/Z_\odot)$. The numbers in brackets next to the age and metallicity measurements are the 1σ confidence limits on the derived values based on 1000 Monte Carlo realizations drawn from a Gaussian distribution of the measurement errors. Note that the Δ's are not well defined for the 0.5 Gyr models in the $D_n(4000)$ vs. Fe4668 that are marked as reliable fits, since the dust-free case cannot be reliably fit.

[a] A check mark, ✓, indicates a reliable fit. Unreliable fits are coded as: "OG" if the point lies off the model grids, "DB" if it lies in the young double-valued Balmer line region, and "DM" if it lies in a degenerate metallicity region (only occurred for the young exponential SFH model in the $D_n(4000)$ – Fe4668 plane).